THE EFFECT OF PROPELLER SLIPSTREAM ON THE STATIC LONGITUDINAL STABILITY AND CONTROL OF MULTI- ENGINED PROPELLER AIRCRAFT

E. Obert
Delft University of Technology
Faculty of Aerospace Engineering
Kluyverweg 1
2629 HS Delft The Netherlands

1. Abstract

A method is presented for the determination of slipstream effects on static longitudinal stability and control of multi-engined propeller aircraft.
The method is partly based on elementary momentum considerations partly on a correlation of windtunnel data. The method allows the determination of:

- o The increase in lift due to propeller slipstream,
- o The change in tail-off pitching moment, both with flaps retracted and deflected.
- o The location of the propeller slipstream relative to the horizontal tailplane and the associated effect on average dynamic pressure at the tailplane.
- o The change in average downwash angle due to slipstream at the tailplane.

For a number of aircraft configurations a comparison is shown between calculated results and windtunnel data.

2. Notation

Symbol	Description	Unit
A_s	Aspect ratio of wing part immersed in the slipstream of a single propeller.	(-)
$A_{s,eff}$	Effective aspect ratio of wing part immersed in the slipstream of a single propeller at low thrust coefficients.	(-)
A_s	Total cross-sectional area of the combined fully contracted slipstream tubes: $\left(A_{s}' = n_e \frac{\pi}{4} D^{*2}\right)$	(m²)
A_W	Wing aspect ratio ($A_W = b^2/S_W$)	(-)
A^*	Cross-sectional area of the part of the outer flow stream tube affected by the slipstream (see Appendix IV).	(m²)
$1+b$	Square-root of the average dynamic pressure ratio at the horizontal tailplane $\left[b = \sqrt{q_h/q} - 1\right]$	(-)
b_s	Width of the tailplane part covered by the slipstream of a single propeller in idealized flow.	(m)
b_w	Wing span.	(m)
c	Wing section chord.	(m)
c'	Extended wing chord (chord extension due to flap deflection).	(m)
$\bar{c}$	Mean aerodynamic chord.	(m)
c_f	Flap chord.	(m)
C_L	Lift coefficient $\left[C_L = \frac{lift}{\frac{1}{2}\rho_o V_o^2 S_W}\right]$	
c_l	Two-dimensional lift curve referred to the extended section chord c'.	(-)
C_{Lp}	Total normal-force coefficient of the combined propellers $\left[C_{L_p} = \frac{n_e N_p}{\frac{1}{2}\rho V_o^2 S_W}\right]$	(-)
$(C_L)_{p-o}$	Power-off lift coefficient.	(-)
ΔC_{Ls}	Lift coefficient due to slipstream deflection by the wing.	(-)
$\Delta C_{Ls,o}$	Lift coefficient due to slipstream deflection by the wing at the zero-lift angle for the wing with flaps retracted. (See fig. 20).	(-)
$\Delta C_{Ls,\alpha}$	Lift coefficient due to slipstream deflection at a given angle-of-attack.	(-)
$c_{ls,o}$	Local lift coefficient at the propeller axis location in the absence of slipstream.	(-)
C_{LT}	Vertical component of total thrust coefficient. $\left[C_T = \frac{T_{tot} \times \sin\alpha_R}{\frac{1}{2}\rho V_o^2 S_W}\right]$	

C_{Lw+s}	Total wing lift coefficient in the presence of slipstream.	
$C_{L\alpha}$	Wing lift curve slope.	(1/deg)
$C_{L\alpha h}$	Horizontal tailplane lift curve slope	(1/deg)
$C_{L\alpha s}$	Lift curve slope of a wing in free air with aspect ratio A_S	(1/deg)
$C_{L\alpha s,eff}$	Lift curve slope of a wing in free air with aspect ratio $A_{s,eff}$	(1/deg)
$c_{l\alpha}$	Airfoil section lift curve slope. - Lift coefficient-versus-angle of attack.	(1/deg)
$c_{l\alpha s}$	Airfoil section lift curve slope at the propeller axis location.	(1/deg)
$c_{l\delta}$	Airfoil section lift curve slope. -Lift coefficient-versus-flap angle	(1/deg)
C_M	Pitching moment coefficient $\left[C_M = \dfrac{M}{\frac{1}{2}\rho V_O^2 S_W \bar{c}}\right]$	(-)
ΔC_{MFS}	Additional pitching moment contribution to the calculated pitching moment due to slipstream C_{Ms} to improve comparison with test data.	(-)
$c_{mo,s}$	Zero-lift pitching moment coefficient of the wing section at the propeller axis location.	(-)
$c'_{m0.25c'}$	Airfoil pitching moment coefficient about the quarter-chord point referred to the extended section chord c'.	(-)
ΔC_{Mp}	Pitching moment coefficient due to total propeller normal force.	(-)
ΔC_{Ms}	(= C_{Ms}) Total pitching moment coefficient due to propeller forces and slipstream.	(-)
c_s	Wing section chord at propeller location.	(m)
ΔC_{MT}	Pitching moment coefficient due to total propeller thrust.	(-)
C_T	Thrust coefficient $\left[C_T = \dfrac{T_{tot}}{\frac{1}{2}\rho V_O^2 S_W}\right]$	
D	Propeller diameter	(m)
D^*	Diameter of fully contracted slipstream.	(m)
Δh^*	The (assumed) vertical displacement of the slipstream centre line due to the propeller axis at the propeller plane not coinciding with the stream-line leading to the forward stagnation point.	(m)
h_{tot}	Total distance in the Z-direction between slipstream centreline and horizontal tailplane.	(m)
Δh_l	Vertical displacement due to angle-of-attack of the quarterchord point of the tailplane section at the propeller location.	(m)
h_t	Vertical distance between the tailplane section at the propeller location and the propeller axis.	(m)
$(\Delta_{ht})_{upw}$	Vertical displacement of slipstream centre line due to upwash in front of the wing due to flap deflection	(m)
$(\Delta h_t)_\alpha$	Vertical displacement of slipstream centre line due to angle-of-attack.	(m)
$(\Delta h_t)_{\delta f}$	Vertical displacement of slip-stream centre line due to flap deflection.	(m)
i_{cs}	Incidence of wing section chord at the propeller location	(deg
L_W	Wing lift not affected by slipstream.	(N)
L_S	Wing lift due to slipstream.	(N)
l_h	Tail arm. (Measured between wing and tailplane quarter-mean-aerodynamic chord points).	(m)
l^*_h	Distance between wing trailing-edge and tailplane quarter-chord points at the propeller axis location.	(m)
K_ε	Downwash factor. ($K_\varepsilon = Z_w/Z_\varepsilon$)	(-)
n_e	Number of propellers.	(-)
N_p	Normal force of a single propeller	(N)
P	Coefficient in downwash formula	(-)
q	(= q_o) Dynamic pressure of the undisturbed flow	(N/m²)
q_h	Average dynamic pressure at the horizontal tailplane.	(N/m²)
q_s	(= q_j) Average dynamic pressure in the fully contracted slipstream.	(N/m²)
S_h	Horizontal tail area.	(m²)
S_s	(= $S_{h,s}$). Area of horizontal tail surface immersed in the idealized slipstream.	
S_w	Wing reference area	(m²)
T_{tot}	(=T) Total propeller thrust	(N)
ΔV	Increase in velocity in the fully contracted slipstream	(m/s)
V_O	Velocity of undisturbed airflow.	(m/s)
X	Coordinate parallel to the fuselage reference line.	(m)
X_{CG}	Centre-of-gravity position along the X-axes.	(m)
$X_{FS}/\bar{c}$	Dimensionless distance over which the lift due to slipstream is assumed to be displaced to obtain calculated pitching moment data due to	

	slipstream with flaps deflected which match with test data.	(-)
X_{prop}	Propeller plane coordinate along the X-axis.	(m)
$X_{0.25cs}$	Quarter-chord coordinate along the X-axis of the wing section at the propeller location.	(m)
Y	Lateral coordinate.	(m)
$Y_{s,o}$	Distance between propeller axis and fuselage centre line.	(m)
Z	Coordinate in the plane of symmetry prependicular tot he fuselage reference line. Positive upward.	(m)
Z_{CG}	Centre-of-gravity position along the Z-axis.	(m)
Z_h	Distance along the Z-axis between the wing trailing-edge and the horizontal tailplane at the propeller axis location.	(m)
Z_1	Distance along the Z-axis between the propeller axis and the wing trailing edge.	(m)
Z_W	Actual vertical displacement of the wing wake relative to the wing trailing edge at the horizontal tailplane position.	(m)
Z_ε	Wing wake displacement calculated with the lifting line theory	(m)
α	Angle-of-attack.	(deg)
α^*	Change in flow direction immediately behind the propeller relative to the direction of the undisturbed flow	(deg)
α_O	Airfoil section zero-lift angle-of-attack.	(deg)
$\Delta\alpha_{o,f}$	Change in airfoil section zero-lift angle-of-attack due to flap deflection.	(deg)
α_R	Angle-of-attack related to the fuselage reference line.	(deg)
α_S	Angle-of-attack of the wing part immersed in the propeller slipstream.	(deg)
$\alpha_{S,eff}$	Effective angle-of-attack of the wing part immersed in the slip stream at low thrust coefficients.	(deg)
δ	(Plain) flap defection angle	(deg)
δ_f	Flap setting.	(deg)
ε	Downwash angle.	(deg)
ε'	Estimated average downwash angle of the flow affected by slipstream.	(deg)
$(\varepsilon_o)_{p\text{-}o}$	The average downwash angle at the horizontal tailplane at zero lift in the power-off condition.	(deg)
	The slope of the downwash-angle versus-lift curve at the power-off condition.	(deg)
ε_S	Calculated downwash angle in the slipstream.	(deg)
$\varepsilon_{\alpha=o}$	Downwash angle at α_R = O at the power-off condition.	(deg)
	The increase in average downwash angle at the tail due to inflow into the slipstream when the slipstream velocity is twice the velocity of the undisturbed flow.	(deg)
ϕ	Angle defined in Appendix IV.	(-)
λ	1: Wing taper ratio 2: Parameter used in ref. 6	(-)
ϱ	Air density.	(kg/m^3)
σ	Parameter defined in Appendix II	(-)
Θ	Slipstream turning angle.	(deg)

3. Introduction

The effect of propeller slipstream on the longitudinal characteristics of an aircraft has caught the attention of aircraft designers since the early days of aviation. In particular on multi-engined aircraft propeller slipstream often leads to a decrease in longitudinal stability and non-linear control characteristics when speed or power setting are varied.
This may severely limit the allowable centre-of-gravity range in particular on high-performance aircraft.
But most of all the unpredictability of slipstream effects is a matter of concern, in particular when no windtunnel data with powered propellers are available for the configuration under consideration.
For preliminary design purposes open literature provides guidelines for the estimation of the effect of propeller slipstream on lift and drag. Tail-off pitching moments, in particular with flaps deflected, downwash at the tail and the location of the slipstream relative to the tail and consequently the average dynamic pressure at the tail with slipstream present are to the author's knowledge not covered in open literature. In the present paper a semi-empirical method is presented which allows the estimation of these parameters. With these data available a first-order estimate of the effect of propeller slipstream on longitudinal stability and control should be possible.

4. Historical Overview

In the '20's and '30's the analysis of propeller slipstream effects was mainly limited to gathering data collections from which some general trends were derived (refs. 1-3). Some relevant work was also performed on the analysis of the characteristics of a two-dimensional model wing placed in an open windtunnel test section. This resembled a wing partly immersed in a slipstream at very low flight speeds (refs. 4, 5).

The first systematic investigation concerning the increase in lift on a multi-engined aircraft due to propeller slipstream was performed by Smelt and Davies in 1936. This resulted in the classic semi-empirical method reported in ref. 6. No configurations with high-lift devices were considered. The method was primarily aimed at conditions with low thrust coefficients. The increase in lift due to slipstream was thought to be primarily caused by an increase in dynamic pressure of the flow about the part of the wing immersed in the slipstream. The downwash was not considered explicitly.

In the late 1930's and early 1940's efforts were made to describe slipstream effects with theoretical models. Numerical values for the required coefficients of proportionality could not be determined however (ref. 7-12). Also more testdata were published (refs. 13, 14).

With the increase in engine power in the 1940's the need for better insight in slipstream effects on aircraft characteristics lead to several systematic windtunnel investigation such as presented in refs. 15-17.

With the advent of the turbojet engine the interest in conventional propeller aircraft disappeared in the 1950's in particular from the research programme's of the large research institutes.

However, in the late 1950's and throughout the 1960's extensive research into the feasibility of V/STOL-aircraft lead to a renewed interest in propellers (refs. 18-32). Because of the emphasis on V/STOL-characteristics most of the research was performed at very low speed (and thus very high thrust coefficients). Also, most configurations investigated (except those of refs. 33-37) had the greater part of the wing immersed in the propeller slipstream. Based on these latter investigations Kuhn (ref. 38,1959) developed a semi-empirical method which allows the estimation of the increase in lift due to propeller slipstream with flaps deflected and at very low flight speeds up to V = 0 .

In ref. 39 some results are presented of the application of the method by Kuhn.
In refs. 40 and 41 more recent analyses are presented of the effect of slipstream on longitudinal characteristics.

Although two oil crises and the deregulation in the US and subsequent developments in airline operation renewed the interest in conventional propeller aircraft no method has been published since then which allows the analysis of the combined slipstream effects on longitudinal aircraft characteristics.

Numerous investigations were performed and reported on propellers and propeller-airframe interaction. These were however mainly aimed at obtaining better insight in details of the flow and at the development of computer codes based on full-potential, Euler or Navier-Stokes flow equations. None of these studies produced results up to now which could be used to determine overall aircraft characteristics.

5. Some remarks on the methods by Smelt and Davies and Kuhn

As mentioned before the method by Smelt and Davies (ref. 6) has the following characteristics:

a. Only clean wings are considered.

b. Only low thrust coefficients are considered

c. The increase in lift due to slipstream can be written as (in the present report's notation):

$$\Delta C_{L_s} = \frac{D^* c_s}{S_W} \Delta V \left[\lambda c_{l_{s,o}} - 0.6\, c_{l_{\alpha s}}(\alpha_R - \alpha^*)\right]$$

In the first term between brackets λ is estimated for two extreme cases:

$\lambda = 2$ when the ratio between slipstream diameter and average chord of the part of the wing immersed in the slipstream is large. This leads effectively to the assumption that the spanwise lift distribution over this part of the wing can be treated as a two-dimensional flow problem.

$\lambda = 1$ when the ratio between slipstream diameter and average chord of the part of the wing in the slipstream is very small. The reasoning behind the latter is rather qualitative.

Comparison with windtunnel data lead to a correlation curve where λ varied between 1 and 1.8 as a function of the aspect ratio of the total part of the wing immersed in the combined slipstreams.

The second term between brackets takes into account the change in local angle-of-attack due to downwash behind the propeller(s). The factor 0.6 is an empirical constant.

Although for very low thrust coefficients the method by Smelt and Davies may in certain cases give reliable results many cases have been reported where the comparison between theory and testdata was unsatisfactory.

The method by Kuhn (ref. 38) approaches the problem from the other side. The starting point is the static condition ($V_0 = 0$) where the lift is entirely determined by the propeller slipstream. Windtunnel test data show that the slipstream momentum is effectively rotated over an angle θ by flap deflection. Although Kuhn suggests that the degree of rotation is a function of the ratio of flap chord and propeller diameter C_f/D the shape of the resultant empirical curve is identical to the curve that gives the ratio of lift curve slopes due do flap deflection and change in angle of attack (see fig. 7). Furthermore a thrust-recovery factor F/T is introduced to incorporate viscous effects. (See fig. Ic, Appendix I).

Having established empirical relations between propeller thrust and the total force on the wing-propeller(s) combination as a function of angle-of-attack and flap deflection for different flap types at static conditions ($V_0=0$) Kuhn then proceeds in formulating a model for the total lift on wing-propeller(s) combinations at low flying speeds.

Basically it is assumed that the total lift on the wing is determined by the vertical component of the outgoing momentum of the stream tubes determined by the propeller diameters and the wing span. The downwash angle of the propeller slipstream behind the wing is assumed to remain equal to the value found for static conditions. Thus no effect of forward speed or thrust coefficient is considered. The downwash angle of the remaining stream tube determined by the wing span is taken according to lifting line theory for the condition with power off:

$$\varepsilon = 57.3 \frac{2C_{L_{P-O}}}{\pi A_W} \quad \text{deg.}$$

As the slipstream turning angle θ is kept constant a correction factor is added to obtain the correct power-off lift when the thrust coefficient approaches $C_T = 0$ and consequently the turning angle θ approaches the power-off downwash angle ε.

Also, a comparison with test data required the addition of a multiplication factor $K = 1.6$ to the calculated extra lift due to slipstream.

Thus, although the method by Kuhn allows the estimation of lift due to propeller slipstream with flaps deflected it shows much room for improvement in particular at lower thrust coefficients.

6. Determination of the effect of propeller slipstream on static longitudinal stability

When at constant speed propeller thrust is increased the total flow condition about an aircraft changes.

Four elements can be distinguished.

1. The wing lift increases.
2. The tail-off pitching moment increases in a negative sense, in particular with flaps deflected.
3. The average downwash angle at the horizontal tail changes.
4. The average dynamic pressure at the horizontal tail changes if the tail is partly immersed in the slipstream.

6.1 The increase in wing lift due to propeller slipstream

Two established methods have been mentioned for the estimation of the increase in wing lift due to propeller slipstream, the methods by Smelt and Davies (ref. 6) and Kuhn. (ref. 38).

In the following a method is presented which offers certain improvements over the methods previously described.

The basic concept is identical to that of the method of ref. 38
The total lift is assumed to be the sum of the vertical components of the outgoing momentum of the stream tubes determined by the fully contracted propeller slipstream and the stream tube determined by the wing span. The cross-sectional area of this latter stream tube is a circle determined by the wing span minus the total cross-sectional area of the fully contracted propeller slipstream. (Fig. 1).

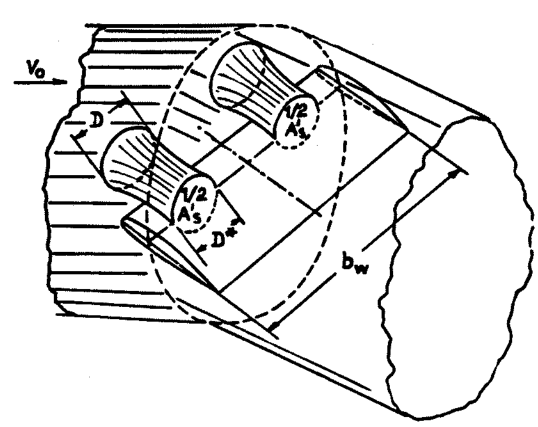

Figure 1 - Lift generation concept.

According to lifting line theory (valid for high-aspect-ratio wings) the turning angle of the stream tube determined by the wing span is equal to the downwash angle:

$$\varepsilon = 57.3 \, \frac{2C_L}{\pi A_W} \quad \text{(deg.)}$$

For very high lift this leads, when the same stream tube analogy is used, to:

$$\sin \varepsilon = \frac{2C_L}{\pi A_W}$$

The lifting theory developed by R.T. Jones (ref. 42) states that for very low aspect ratios ($A \leq 1$) the same expression is valid. However, in this case the lift-curve slope, when the wing aspect ratio approaches zero, can be written as:

$$C_{L_\alpha} = \frac{1}{57,3} \times \frac{\pi}{2} A_W \quad \text{(per deg.)}$$

and

$$C_L = C_{L_\alpha} \times \alpha = \frac{1}{57.3} \times \frac{\pi}{2} A_W \times \alpha \quad \text{(per deg.)}$$

or, for very high angles-of-attack:

$$C_L = \frac{\pi}{2} A_W \sin \alpha$$

Thus: $\sin \varepsilon = \sin \alpha$
and $\varepsilon = \alpha$

Stepniewsky (ref. 44 page 13) suggested that at least for clean wings for higher thrust coefficients the increase in lift due to slipstream could be estimated by considering the flow of the slipstream over the wing to be equivalent to the flow about a wing in a free stream of which the span was equal to the diameter of the fully contracted slipstream and the chord equal to the actual wing's chord at the propeller axis.

The dynamic pressure to be considered is equal to the dynamic pressure in the slipstream and the angle of attack α_S should be measured between the airfoil section's zero-lift angle-of-attack and the centre-line of the propeller slipstream. On a propeller at a given angle-of-attack the latter means that with increasing thrust coefficient the slipstream is deflected more downward and the angle-of-attack α_S of the equivalent wing decreases.

The validity of this concept was first checked on the test data from ref. 28.
In front of a wing, spanning the windtunnel test section a propeller was fitted driven by an electric motor. The propeller and electric motor were mounted separately and were physically detached from the 2-d wing model. The model was constructed such that spanwise lift distribution coul be measured directly. With the propeller in a fixed position the angle of attack of the model could be varied.

Because the model extended from wall to wall in the test section the "free-air" lift could not be determined on the basis of a stream tube being deflected over an angle ε. The downwash angle was taken as zero. Then the lift due to slipstream was taken as:

$$L_S = \rho \, (V_0 + \Delta V)^2 \, \frac{\pi}{4} D^{*2} \sin \varepsilon_S$$

or

$$L_S = \rho \, (V_0 + \Delta V)^2 \, \frac{\pi}{4} D^{*2} \sin \alpha_S$$

As the propeller was fixed $\alpha_S = \alpha$
The test data of ref. 28 and the calculated data obtained according to the procedure outlined above are presented Appendix II and in fig. 11.

This comparison shows that the principle is proved although the effect of varying angle-of-attack is not incorporated in the calculation method. It is unclear if this is a viscous effect or if it is more fundamental.

The increase in lift due to slipstream was then calculated according to the method described for a number of aircraft configurations for which data were available.
Figs. 2-6 show measured and calculated lift curves at various thrust coefficients for some of the clean wing configurations analysed. Ref. 49 presents a more extensive overvieuw.
Fig. 7 shows that in general a comparison between test data and calculated data for the increase in lift due to slipstream on wings without flaps shows

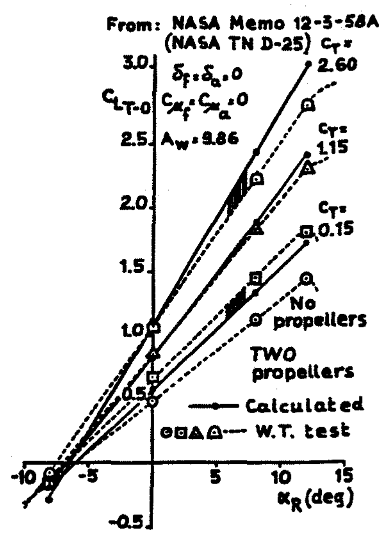

Figure 2 - Lift curves. Configuration ref. 35 with clean wing.

satisfactory results and that no correction factors need be applied.

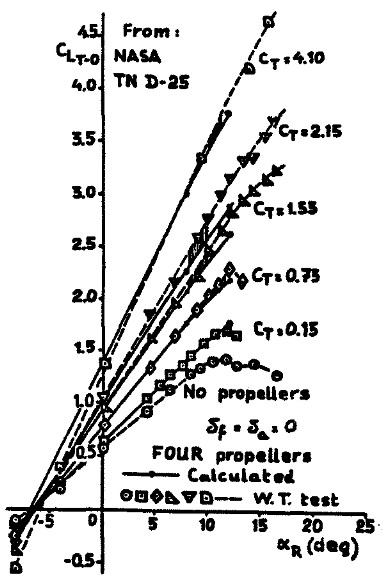

Figure 3 - Lift curves. Configuration of ref. 36 with clean wing.

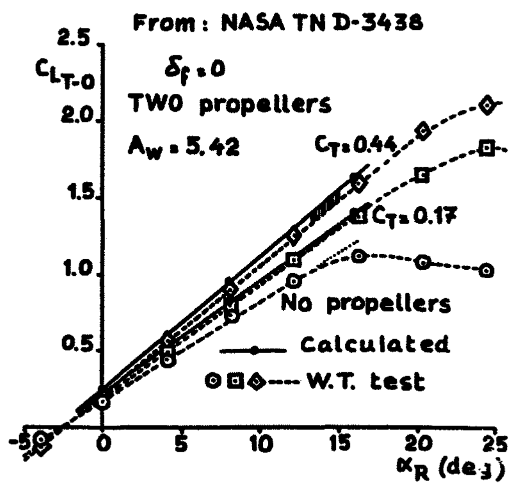

Figure 4 - Lift curves. Configuration of ref. 21 with clean wing.

As mentioned before, in ref. 38 a relation is suggested for wings with flaps deflected between the slipstream turning angle ϴ per degree of flap deflection at zero flight speed (ϴ/δ) and the ratio between flap chord and propeller diameter (c_f/D). This relation is, however, identical to the relation between the ratio of the slope of the lift curves due to flap deflection and due to change in angle-of-attack ($C_{l\delta}/C_{l\alpha}$) as a function of flap-chord-to-section chord ratio (fig. 8). (In the test data considered the propeller diameter was roughly equal to the wing chord).

In the present analysis the latter relation is taken as more relevant. This allows the model previously described for plain wings to be extended to wings with flaps.
This is not strictly in line with a later extension of Jones's theory for small-aspect-ratio wings (ref. 43) which states that when the aspect ratio approaches zero the lift on a flapped wing is determined only by the inclination of the trailing edge of the camber line i.e. the sum of angle-of-attack and flap angle. The theory of ref. 43 was developed for small angles only however. Also the approach as described above produces data far more in line with experimental results.

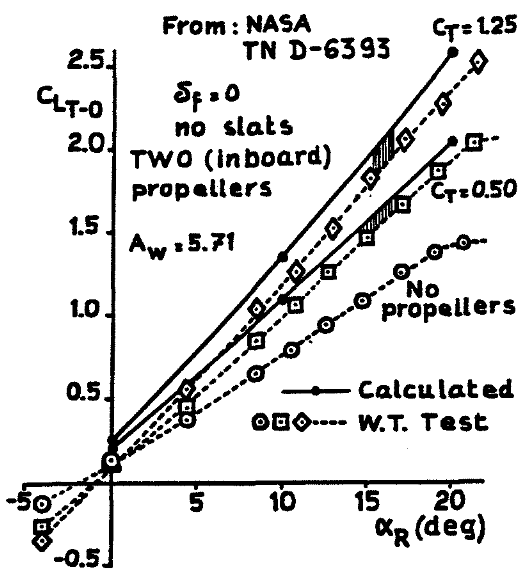

Figure 5 - Lift curves. Configuration of ref. 23 with clean wing.

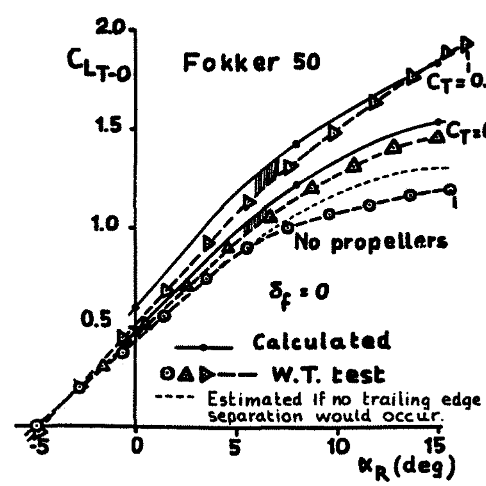

Figure 6 - Lift curves. Fokker 50 with clean wing.

Again it is assumed that the lift due to slipstream is equal to the lift on a wing in free flow with a span equal to the diameter of the fully contracted slipstream and an airfoil section equal to the wing section at the propeller axes with flaps deflected. The angle of attack α_S is measured between the zero-lift angle-of-attack with flaps deflected and the effective propeller slipstream centre line.

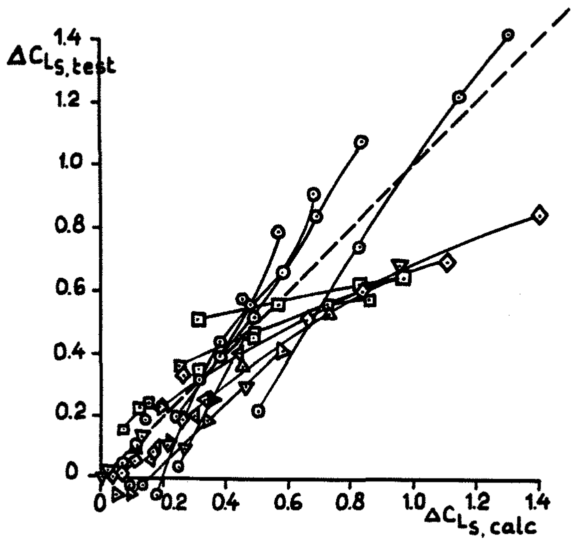

Figure 7 - Increase in wing lift due to slipstream. A comparison between calculated and windtunnel test data.
Flaps retracted.

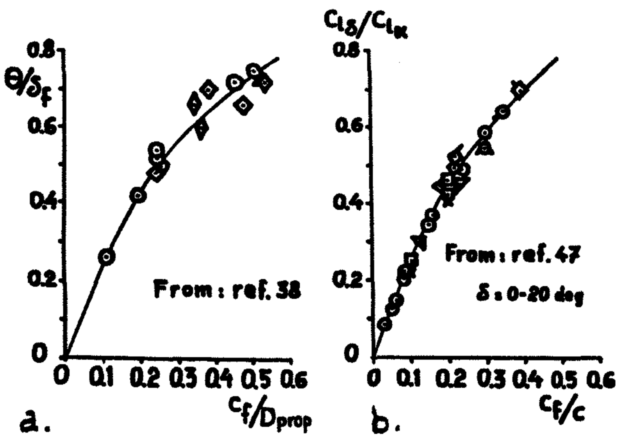

Figure 8 a. slipstream turning angle per degree flap angle versus the flap-chord-to-propeller diameter ratio.

b. $C_{l\delta}/C_{l\alpha}$ versus flap-chord-to-wing-section-chord ratio.

In figs. 12-16 examples are presented of the lift curves for several aircraft configurations with flaps deflected and varying thrust coefficient.

In fig. 17 the measured and calculated increase in lift due to slipstream is compared for a number of aircraft configuration. Note that nu correction factor is required in the calculation procedure.

Many more examples can be found in ref. 49.

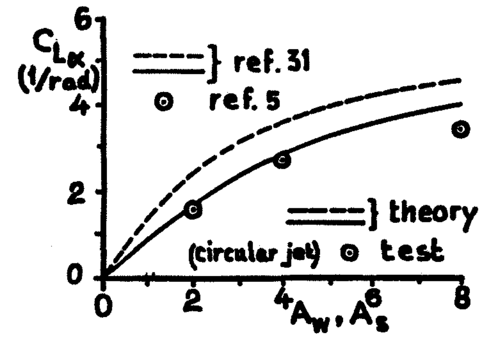

Figure 9 - The lift curve slope of a wing in free air and in a free jet.

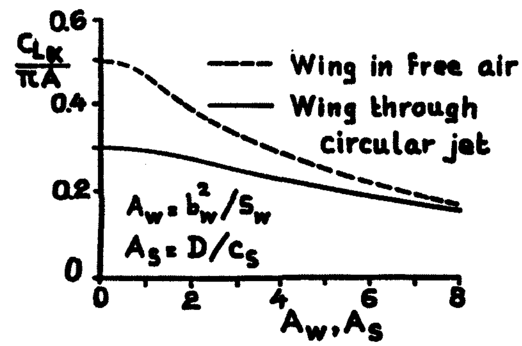

Figure 10 - The lift curve slope $C_{L\alpha}$ devided by π A for a wing in free air and in a free jet.

Up to now fairly high thrust coefficients have been considered. It will be clear that when the thrust coefficient approaches zero the assumption

$$\sin \varepsilon_S = \sin \alpha_S$$

can no longer be maintained.
Following the suggestion from ref. 44 to assume an arbitrary fairing function for the downwash angle ε_S the (slightly modified) function from ref. 44 was adopted. Here the gradual change from $\varepsilon_S = \alpha_S$ to ε was accomplished by considering an imaginary aspect ratio:

$$A_{S_{eff}} = A_S + (A_W - A_S)\left[\frac{V_0}{V_0 + \Delta V}\right]^{(A_W - A_S)}$$

such that

$$\sin \varepsilon_S = \frac{2 C_{L_{\alpha_S}} \times \sin \alpha_S}{\pi A_{S_{eff}}}$$

where $C_{L_{\alpha s}}$ is related to $A_{S_{eff}}$.

A derivation of the formulae used in the calculations is presented in Appendix I.

In the method just described the lift due to slipstream has been compared to the lift of a wing with small aspect ratio.
In refs. 5, 28, 31 the lift due to slipstream at zero flight speed has been analysed both theoretically and experimentally. The results obtained in these investigations indicate that when zero flight speed is approached this assumption seems no longer to hold (figs. 9, 10). This is also suggested by the data of fig. 10 when σ approaches 1 and thus q_S/q_O approaches infinity. For practical values of the thrust coefficient the approach followed produces satisfactory results however.

In the foregoing it has been assumed that the vertical position of the propeller axis does not affect the lift due to slipstream. This assumption is valid when the propeller axis is not more than 0.5 propeller diameter above or below the wing chord (fig. 18). However, recent wind tunnel tests performed at the Delft University of Technology suggest that at more extreme positions large variations in lift can occur. This will be reported on in the near future.

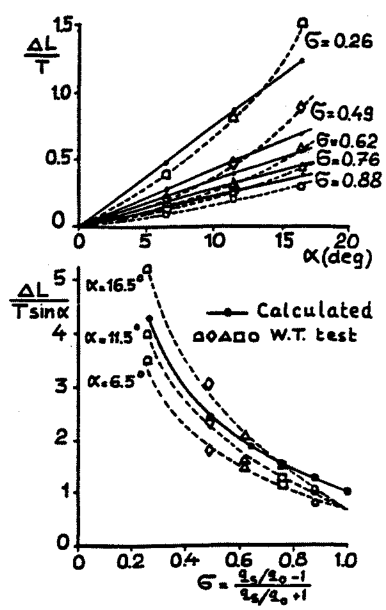

Figure 11 - The lift due to slipstream as a function of the dynamic pressure ratio of slipstream and free flow.

6.2 Change in tail-off pitching moment due to propeller slipstream

For clean wings the effect of slipstream on the tail-off pitching moment of an aircraft is limited to a term:

$$C_{M_{S,O}} = n_e \frac{D^* c_S}{S_W} c_{m_{O,S}} \left[\frac{V_O + \Delta V}{V_O}\right]^2$$

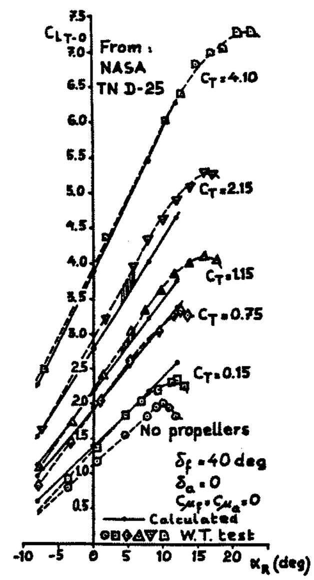

Figure 12 - Lift curves. Configuration of ref. 36 with flaps deflected 40 deg.

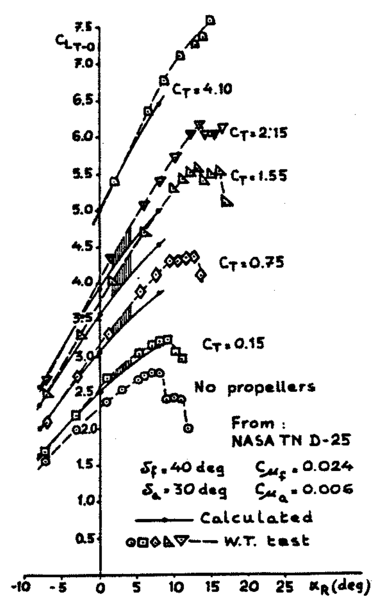

Figure 13 - Lift curves. Configuration of ref. 36 with flaps deflected 40 deg and ailerons 30 deg.

Windtunnel tests show that on clean wings the additional lift due to slipstream applies at the quarter-chord point of the wing section at the propeller axis.

With flaps deflected the situation is different. Glauert has shown in ref. 45 (see also ref. 46, p. 215) a relation between the increase in lift due to flap deflection and the change in pitching moment at constant angle-of-attack (see fig. 19a). This relation derived for potential flow is valid for small flap angles only and can be approximated by the formula:

$$\left[\frac{dc'_{m_{0.25c'}}}{dc'_l}\right]_{\alpha=const.} = -0.25+0.32\frac{c_f}{c'}$$

where c'_m, c'_l and c' refer to the extended chord when flap deflection also leads to chord extension.

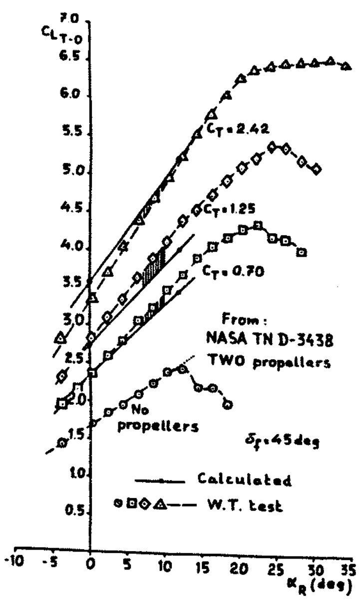

Figure 14 - Lift curves. Configuration of ref. 21 with flaps deflected 45 deg.

Numerous windtunnel tests have shown that in viscous flow the pitching moment is more negative.
Good correlation with test data is obtained by the following modified formula (see fig. 19b):

$$\left[\frac{dc'_{m_{0.25c'}}}{d\,C'_l}\right]_{\alpha=\,const.} = (-0.25+0.32\frac{c_f}{c'})$$

$$\times\ (1\ +\ 0.2\ (1\ -\ \sqrt{2}\ \sin\ \delta_f)$$

In this formula the reference length c' is the extended chord and the moment reference point is also referred to this extended chord. If the reference length is the chord of the airfoil section with flap retracted c and the pitching moment is taken about the 0.25c-point this formula should be written as:

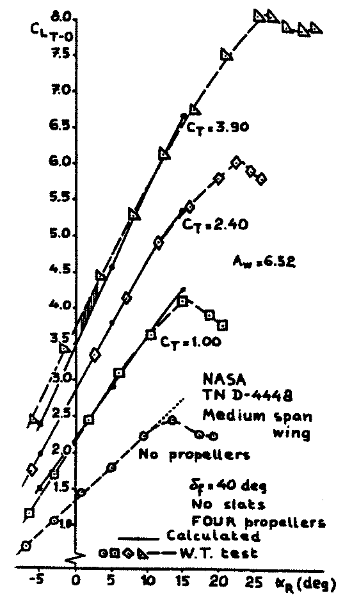

Figure 15 - Lift curves. Configuration of ref. 22 with flaps deflected 40 deg.

$$\left[\frac{dc_{m_{0.25c}}}{dc_l}\right]_{\alpha=const.} = \frac{c'}{c}\left[-0.25+0.32\frac{c_f}{c'}\right]$$

$$\times\left[1+0.2(1-\sqrt{2}\sin\delta_f)\right]-\ 0.25\left[\frac{c'}{c}-1\right]$$

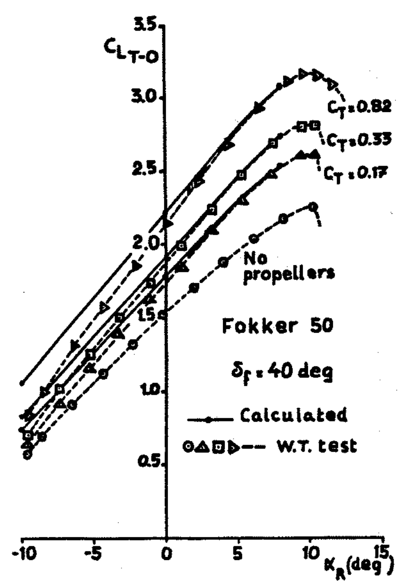

Figure 16 - Lift curves of Fokker 50. Flaps deflected 40 deg.

For a cambered airfoil this increase in pitching moment due to flap deflection and extension should be considered at the zero-lift angle-of-attack for the clean airfoil in order to distinguish between flap effects and angle-off-attack effects.
In the present calculation procedure (fig. 20) for a

tail-off aircraft configuration the zero-lift angle for this configuration is taken.
At other angles-of-attack an extra change in pitching moment occurs due to a change in lift. This extra lift is assumed to apply at 25 percent of the extended chord c'.
Thus:

$$\left[\frac{dc_{m_{0.25c}}}{dc_l}\right]_{\delta_f = const.} = -\Delta c_l \times 0.25\left(\frac{c'}{c}-1\right)$$

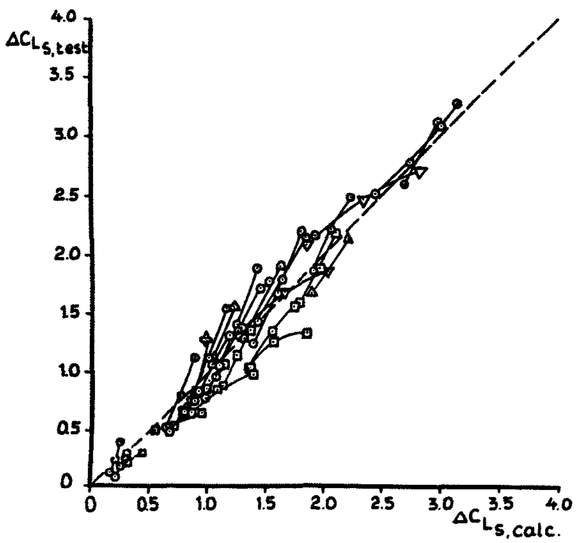

Figure 17 - Increase in wing lift due to slipstream. A comparison between calculated and wintunnel test data. Flaps extended.

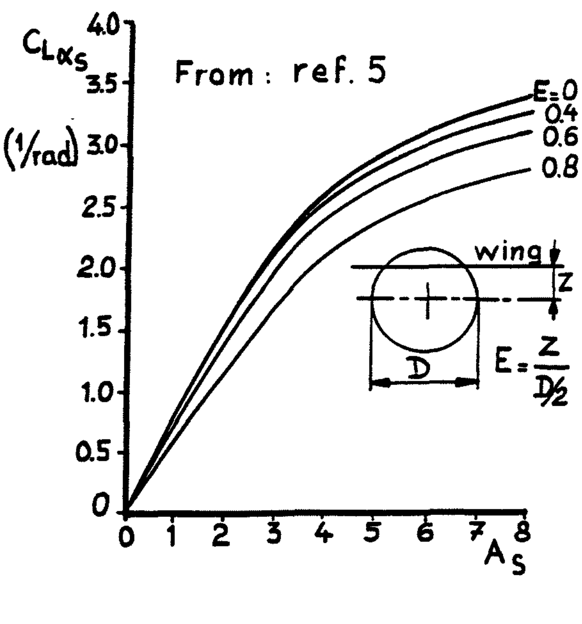

Figure 18 - Effect of the relative jet position on the lift of a wing in a free jet.

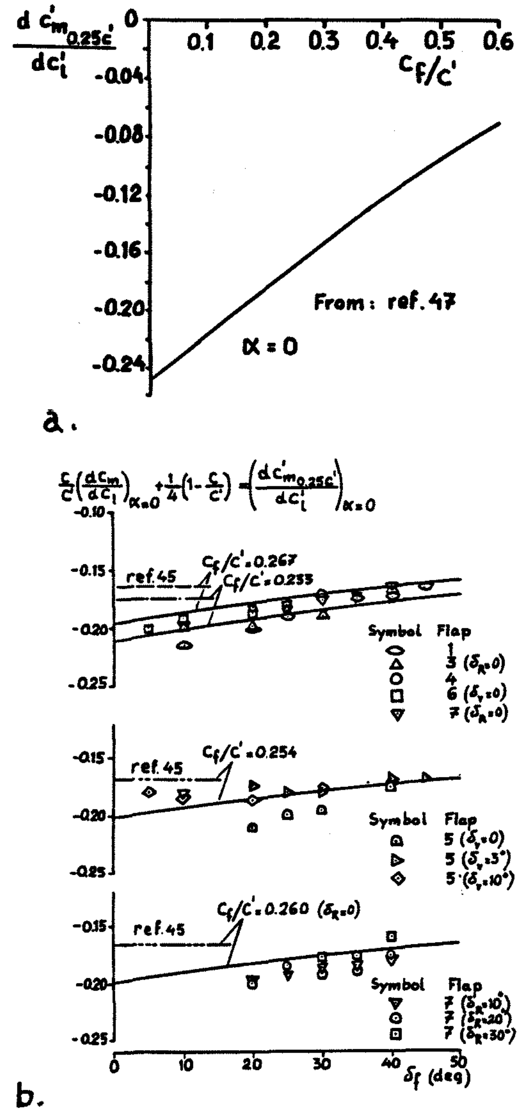

Figure 19 - The effect of the flap-chord-to-airfoil-section-chord ratio on the pitching moment due to flap deflection.
a. From Glauert's theory.
b. Windtunnel test data.

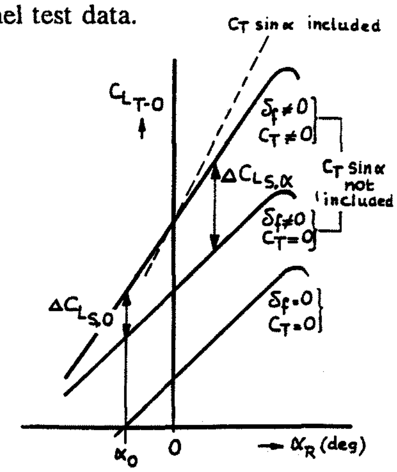

Figure 20 - Definition of $\Delta C_{L_{s,o}}$ and $\Delta C_{L_{s,\alpha}}$ and α_0 (3-dim).

It is now assumed that the lift due to slipstream produces a change in pitching moment according to the same relations as apply to free stream conditions This idea was first suggested in ref. 50.
Thus:

$$[\Delta C_{M_s}]_{\delta_f = const.} = \frac{c'}{c}\left[-0.25 + 0.32\,\frac{c_f}{c'}\right]$$

$$\times[1\times 0.2(1-\sqrt{2}\sin\delta_f)]\,\Delta C_{L_{s,o}} -$$

$$-0.25\left[\frac{c'}{c}-1\right]\Delta C_{L_{s,\alpha}}$$

If the moment reference centre differs from the quarter-chord point an extra change in pitching moment should be added:

$$\Delta C_{M_s} = \frac{X_{CG} - X_{0.25c_s}}{\bar{c}} \times \Delta C_{L_{s,\alpha}}$$

Furthermore, both the direct thrust force and the propeller normal force produce pitching moment contributions:

$$\Delta C_{M_T} = -\frac{Z_T - Z_{CG}}{\bar{c}} \times C_{T_{eff}}$$ (For definition of $C_{T_{eff}}$ see App. V)

$$\Delta C_{M_P} = \frac{X_{CG} - X_{prop}}{\bar{c}} \times C_{L_P}$$

The determination of C_{L_P} is covered in ref. 24 (see also Appendix I).
Finally, a comparison was made between the sum of the pitching moment contributions described above and test data. The difference was assumed to be caused by a shift in the point op application of the wing lift due to slipstream.

$$\Delta C_{M_{FS}} = [C_{M_{S,test}} - C_{M_{S,calc}}] = -\frac{\Delta X_{FS}}{\bar{c}}\,\Delta C_{L_{S,\alpha}}$$

$\Delta X_{FS}/\bar{c}$ has been determined for a large number of configurations and test conditions. Fig. 21 shows representative examples and the curve faired through the data points. The curve adopted is:

$$\frac{\Delta X_{FS}}{\bar{c}} = 0.05 + 0.5\left[\frac{c'}{c}-1\right]$$

The total change in pitching moment coefficient due to operating propellers on a tail-off aircraft configuration can then be described as:

$$[C_{M_s}]_{\alpha = const.} = \frac{c'}{c}\left[-0.25 + 0.32\,\frac{c_f}{c}\right]$$

$$\times\,[1+0.2\,(1-\sqrt{2}\,\sin\delta_f)]\,\Delta C_{L_{s,o}}$$

$$+\left[-0.25\,(\frac{c'}{c}-1) + \frac{X_{CG} - X_{0.25c_s}}{\bar{c}}\right]\Delta C_{L_{s,\alpha}}$$

$$+\ \frac{X_{CG} - X_{prop}}{\bar{c}}\,C_{L_P} - \frac{Z_T - Z_{CG}}{\bar{c}}\,C_T$$

$$-\left[0.05 + 0.5\,(\frac{c'}{c}-1)\right]\Delta C_{L_{s,\alpha}}$$

Examples of tail-off pitching moment curves for configurations with running propellers at different thrust coefficients, both as calculated and as obtained from windtunnel tests are presented in figs. 22-26.

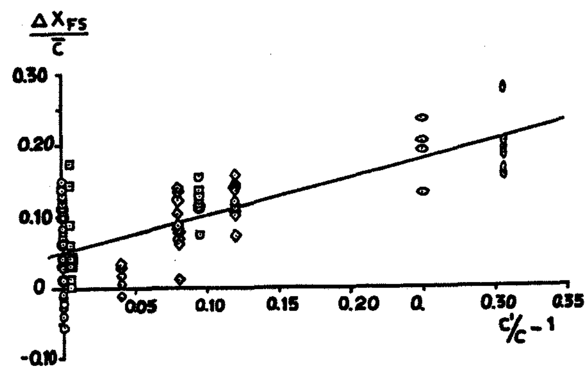

Figure 21 - Assumed shift in point of application of lift due to slipstream to improve the correlation between calculated and measured pitching moment changes due to propeller slipstream.

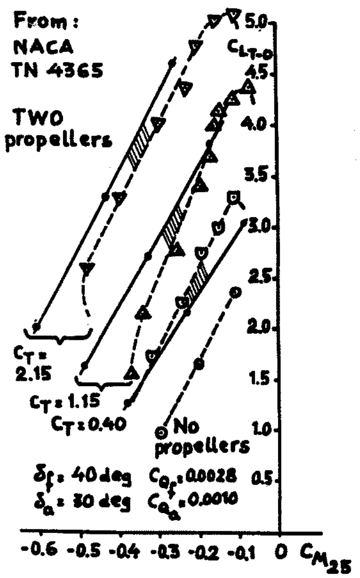

Figure 22 - Tail-off pitching moment curves. Configuration of refs. 34 and 35. Flaps deflected 40 deg and ailerons 30 deg.

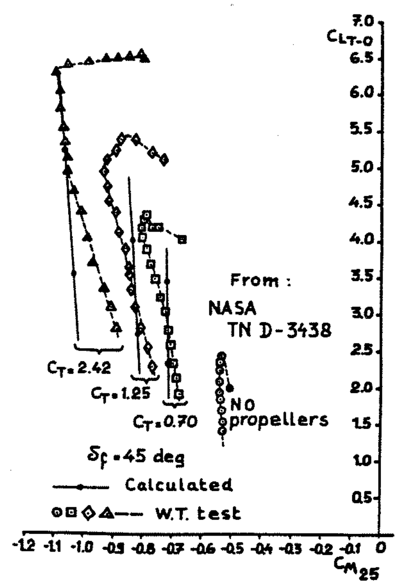

Figure 24 - Tail-off pitching moment curves. Configuration of ref. 21. Flaps deflected 45 deg.

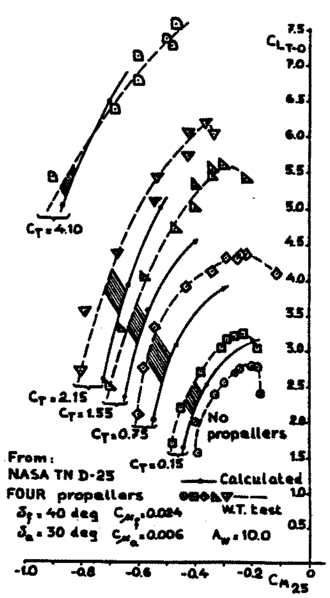

Figure 23 - Tail-off pitching moment curves. Configuration of ref. 36. Flaps deflected 40 deg. and ailerons 30 deg.

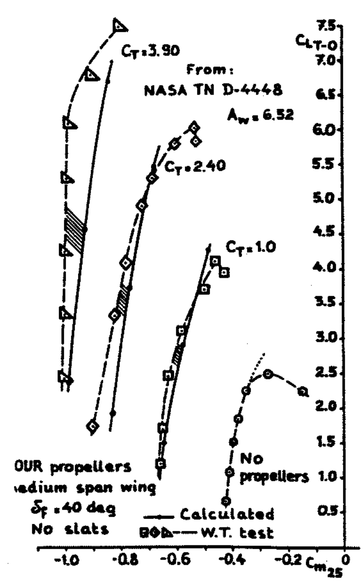

Figure 25 - Tail-off pitching moment curves. Configuration of ref. 22. Flaps deflected 40 deg.

6.3 <u>The vertical position of the slipstream centre lines</u>

When lift due to slipstream was discussed in chapter 6.1 the average downwash angle for slipstream and the outer flow were assumed to have different values ε_S and ε with no interaction between the two flows.

Measured average downwash angles at tailplane locations sufficiently far above the propeller slipstream show however (to a first order) a unique linear relationship between average downwash angle and total lift coefficient.

Whether high lift is generated by a high angle-of-attack, a very efficient flap system or by propeller slipstream, rougly the same C_L -versus - ε curve is found (see figs. 27, 28).

Apparently, the interaction between slipstream and outer flow is such that, at least in the region of convential horizontal tail surfaces slipstream and outer flow can be considered as if they produce the same average downwash angle in the part of the outer flow stream tube between the outboard edges of the propeller slipstream tubes.

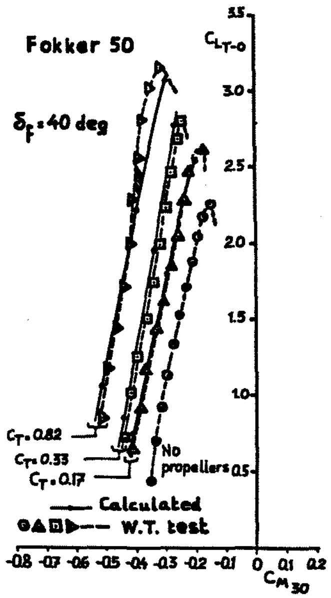

Figure 26 - Tail-off pitching moment curves. Fokker 50. Flaps deflected 40 deg.

As a check the following analysis was performed:

In fig. 29 a cross section of the idealised flow behind a wing with two propellers is shown. The flow is assumed to consist of two stream tubes defined by the fully contracted propeller slipstream and the outer flow stream tube. In Appendix IV the formulae used in the analysis have been derived.

It is now assumed that the vertical components of the outgoing momentum of the flow through area A* (with downwash angle ε) and of the slipstream with total area $A'_S = 2 \times \pi/4 \, D^{*2}$ and downwash angle ε_S can be combined into the vertical component of a total momentum with different velocities but a single downwash angle ε'.
with

$$\sin\varepsilon = \frac{\rho V_0^2 A^* \sin\varepsilon + \rho \, (V_0 + \Delta V)^2 A'_s \sin\varepsilon_s}{\rho V_0^2 A^* + \rho \, (V_0 + \Delta V)^2 A'_s}$$

With the above equation and some of the formulae from Appendix I the downwash angle ε' has been calculated for a number of aircraft configurations. As an example ε' versus C_L for the configuration of ref. 36 with the flaps deflected to 60 deg and the ailerons to 30 deg for thrust coefficients $C_T = 0$ and $C_T = 2.15$ is presented in fig. 30.

Thus, the assumption that the average downwash far behind the wing is only dependent on the total lift coefficient, irrespective of the way this lift coefficient is achieved seems to hold.

In real flow the downwash angle, averaged over the tailplane's span is dependent on the height above the wing wake.
Fig. 31 shows that:

$$\varepsilon = 57.3 \frac{P \, C_L}{\pi \, A_W}$$

where P varies on average between 1.5 and 2.5. When it is assumed that this relation also applies with propeller slipstream present it follows that with engines mounted on the wing the centre line of the slipstream should show a downwash angle corresponding tot a value for P close to 2.5. Varying P between 2.5 and 2.0 showed best correspondence with test values for P = 2.2.

So, far behind the wing the inclination of the slipstream centre line is:

$$\varepsilon_{S,CL} = 57.3 \times \frac{2.2 \, C_L}{\pi \, A_W}$$

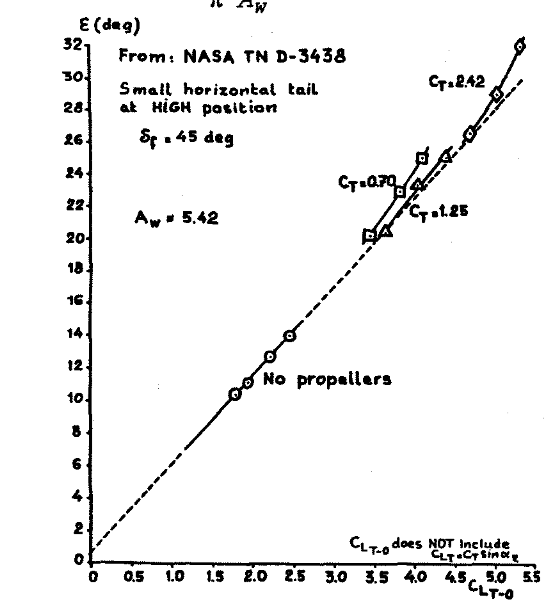

Figure 27 - Downwash angle-versus-lift. Configuration of ref. 21. Flaps deflected 45 deg.

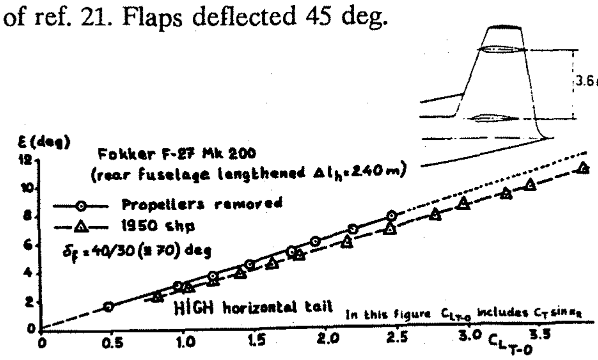

Figure 28 - Downwash angle-versus lift. Fokker F-27 model with high tail. Double-slotted flap deflected 70 deg.

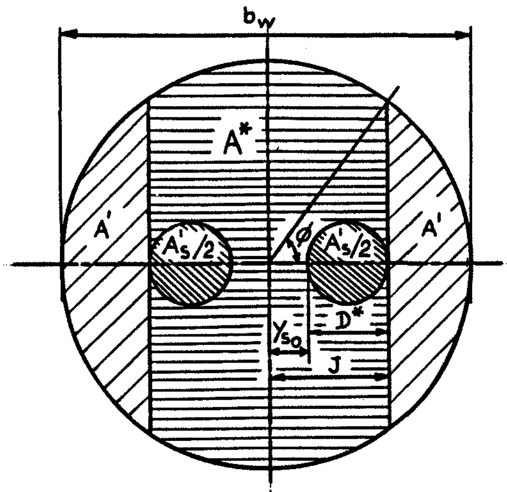

Figure 29 - Idealised cross section of flow over a wing with propeller slipstream.

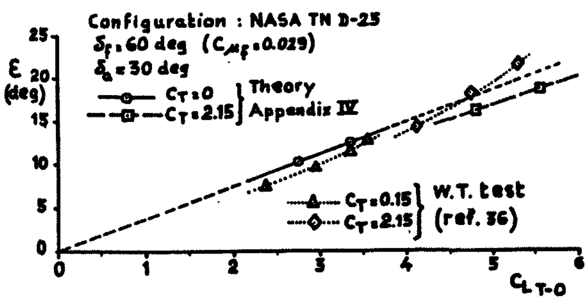

Figure 30 - Effect of propeller slipstream on downwash. Comparison between theory and experiment.

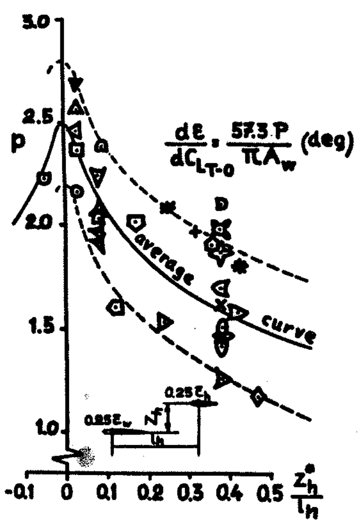

Figure 31 - Effect of tailplane height above the wing plane on downwash gradient.

In particular at high lift coefficients the wing wake is not flat but curved with a higher downwash angle near the wing trailing edge.

For a straight wing with $A_W = 8$ and taper ratio $\lambda = 0.3$ the flow field has been calculated for $C_L = 1$, 2 and 3.
Fig. 32a shows the flow field for $C_L = 2$. The vertical displacement of the wake relative to the wing trailing edge Z_W is clearly larger than $Z_\varepsilon = l_h \sin \varepsilon$. The ratio $K_\varepsilon = Z_W/Z_\varepsilon$ as a function of l_h/c_s as derived from the analysis mentioned above is presented in fig. 32b. It is assumed to be valid for wing aspect ratio's $5 < A_W < 14$. Fig. 35 shows that $K_\varepsilon \approx 1.5$ when $l_h/c_s = 3.0$ to 4.0 .

With the data from fig. 32b the slipstream centre line can be determined for clean wings when the propeller axis lies on or close to the streamline that leads to the forward stagnation point on the airfoil. The slipstream centre line coincides, in the present model, with the wing wake.

The vertical distance between the horizontal tail surface and the slipstream centre line is than the sum of the geometrical distance between the tail surface and the propeller axis (h_t) at zero angle-of-attack, the vertical displacement of the slipstream centre line (or wing wake) passing through (or assuming its origin at) the clean wing's trailing edge (Δh_ε) and the vertical displacement of the horizontal tail due to angle of attack (Δh_l):

$$h_t = Z_h - Z_T$$

$$\Delta h_\varepsilon = l_h^* \times tg\left[K_\varepsilon \frac{d\varepsilon}{dC_L}\frac{dC_L}{d\alpha}\alpha_R + K_\varepsilon \frac{d\varepsilon}{dC_L}\Delta C_{L_s} + K_\varepsilon \varepsilon_{\alpha=0}\right]$$

$$\Delta h_l = -l_h \, tg\, \alpha_R$$

where l_h = distance from wing quarter-chord point to tailplane quarter-chord point.
l_h^* = distance from wing trailing edge to tailplane quarter chord point.

On most aircraft configurations the propeller axis is situated above or below the wing chord plane at a distance Z_T and is located 0.50 c_S to 1.00 c_S in front of the wing. Also when the angle-of-attack increases the propeller centre line moves up. When flaps are deflected the streamline leading to the forward stagnation point moves down with respect to the propeller axis.

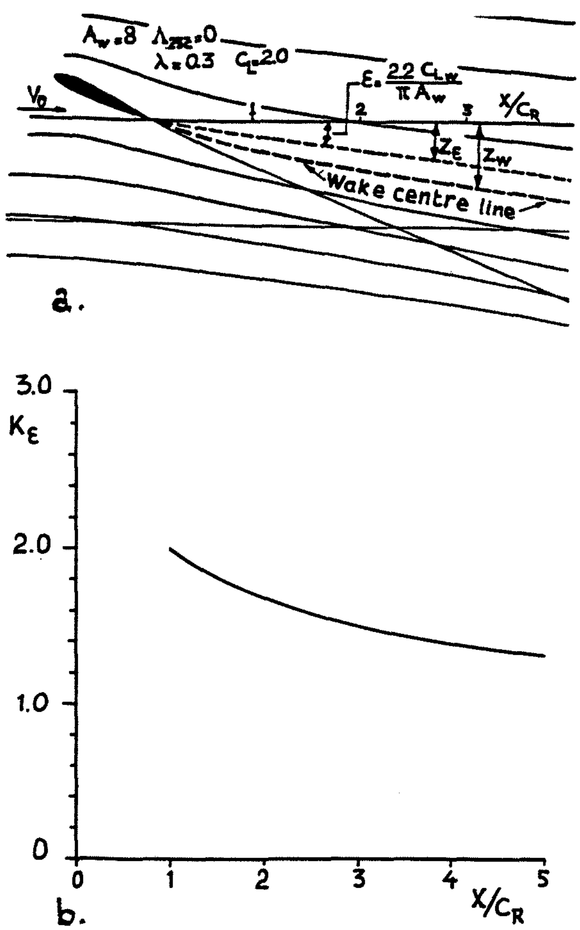

Figure 32 - Shape and position of wing wake.
a. Typical example of flow condition.
b. Kε versus distance behind the wing trailing edge.

In all these cases the slipstream centre line will not coincide with the wing wake.

In the present analysis it is assumed that the slipstream centre line is off-set from the wing wake for a clean wing at the same C_L over a constant distance Δh^* . This distance is the sum of (see fig. 33):

1. $(\Delta h_t)_\alpha$: The (upward) vertical displacement of the propeller disc centre due to angle-of-attack.

$$(\Delta h_t)_\alpha = -(X_{0.25c_s} - X_{prop}) \sin \alpha_R$$

2. $(\Delta h_t)_{\delta f}$: The (downward) vertical displacement of the wing trailing-edge when the flaps are deflected.

$$(\Delta h_t)_{\delta_f} = c_f \times \sin \delta_f$$

3. $(\Delta h_t)_{upw}$: The (upward) vertical displacement due to flap deflection of the streamline running through the propeller disc centre between the propeller and the quarterchord point on the airfoil.

$$(\Delta h_t)_{upw} = +0.25[X_{0.25c_s} - X_{prop}] \sin \Delta \alpha_{0,f}$$

The coefficient 0.25 was chosen somewhat arbitrarily after regarding the streamline pattern about a number of airfoil configurations such as presented in fig. 33.

The vertical displacement of the wing trailing edge relative to the propeller due to angle-of-attack is assumed to be compensated by an increased upwash of the slipstream between the propeller and the airfoil quarter-chord point.

The total vertical displacement of the slipstream can be written as:

$$\Delta h^* = (\Delta h_t)_\alpha + (\Delta h_t)_{\delta_f} + (\Delta h_t)_{upw}$$

The total height of the horizontal tail surface above the slipstream centre line can then be written as:

$$h_{tot} = h_t + \Delta h_\varepsilon + \Delta h_l + \Delta h^*$$

or:

$$h_{tot} = h_t$$

$$+ l_h^* \, tg\left[K_\varepsilon \frac{d\varepsilon}{dC_L} \frac{dC_L}{d\alpha} \alpha_R + K_\varepsilon \frac{d\varepsilon}{dC_L} \Delta C_{L_s} + K_\varepsilon \varepsilon_{\alpha=0}\right]$$

$$- l_h \, tg \alpha_R - [X_{0.25c_s} - X_{prop}] \sin \alpha_R$$

$$+ C_f \sin \delta_f - 0.25(X_{0.25c_s} - X_{prop}) \sin \Delta \alpha_{0,f}$$

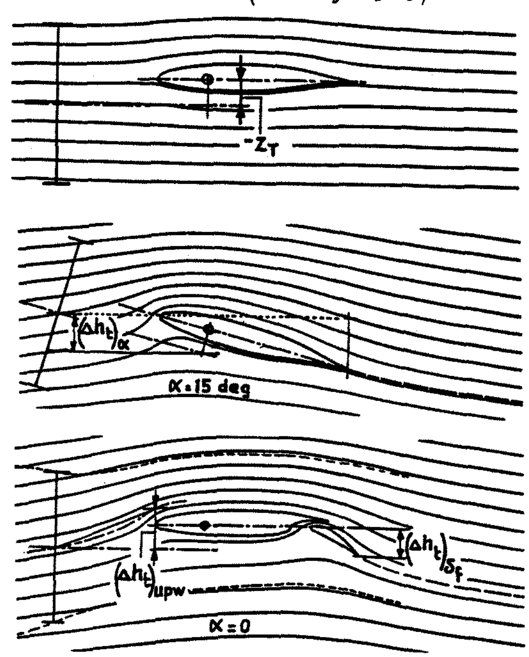

Figure 33 - The vertical displacement of the slipstream centre line due to angle-of-attack and flap deflection.

6.4 The average dynamic pressure at the horizontal tailplane

A model has now been established for the propeller slipstream centre line shape and location. If it is assumed that the slipstream cross section remains circular with diameter D^* and that no mixing with the outer flow or deformation occurs the position of the propeller slipstream relative to the horizontal tail surface can then be determined.

It is further assumed that:

a. Slipstream rotation and resultant lateral translation of the slipstream can be neglected. Handed propellers are not considered.

b. On configurations with more than two engines (four or six) only the two inboard engines affect the flow over the tail.

The average dynamic pressure at the tail can now be determined as a function of the vertical distance between the tail surface and the slipstream centre line and of the ratio between slipstream diameter and tailspan.

As shown in Appendix III the average dynamic pressure can then be written as:

$$\frac{q_h}{q} = \left[1 + \left(\frac{\Delta V}{V_o}\right)_{AV}\right]^2 = (1+b)^2$$
$$= \left[1 + \frac{\Delta V}{V_o}\right]^2 \frac{S_{h,s}}{S_h} + \frac{S_h - S_{h,s}}{S_h}$$

where:

$$\frac{S_{h,s}}{S_h} = \frac{2 \times c_s}{S_h} \times D^* \sqrt{1 - \left[\frac{h_{tot}}{D^*/2}\right]^2}$$

In ref. 16 a detailed windtunnel test programme is reported where on a four-engined aircraft model downwash and average dynamic pressure at the tail were investigated for a large number of tailplane positions relative to the wing both with single- and counter-rotating propellers and both with split flaps retracted and deflected 60 degrees.
For this configuration the slipstream location for the inboard engines and the average dynamic pressure at the tail has been determined according to the procedure indicated above for a thrust coefficient $T_C = 0.40$.
$\Delta V/V_o$ ($= b$) as a function of $h_{tot}/D^*/2$ as calculated is shown as a dotted line in fig. 34.

Figure 34 also shows test data on $\Delta V/V_o$ as derived from ref. 16 again plotted versus the calculated relative slipstream centre line position. The test data substantiate the assumptions concerning the relative position of the slipstream centre line.
However the average dynamic pressure starts to increase at larger distances between tailplane and slipstream centre line than indicated by the dotted line. This indicates that the assumption that no mixing between slipstream and outer flow or that no deformation occurs does not hold.
Mixing and possibly also deformation apparently does occur with consequently a widening of the slipstream.

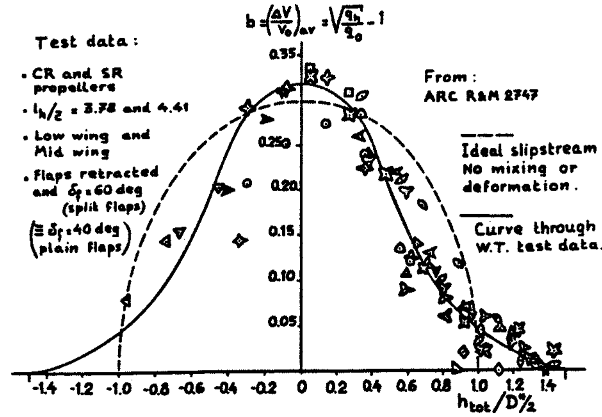

Figure 34 - Effect of slipstream position on average dynamic pressure at the horizontal tailplane. Comparison between theory and experiment.

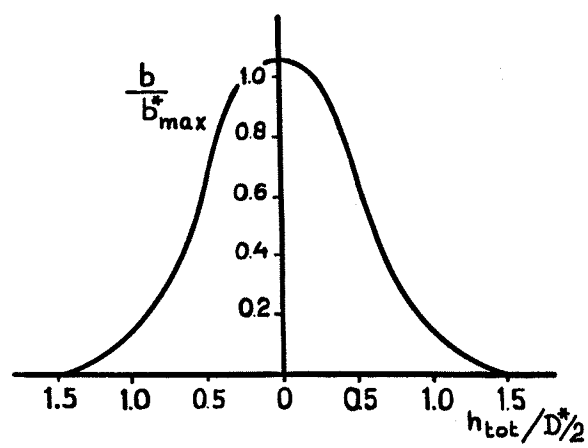

Figure 35 - Effect of slipstream position on average dynamic pressure at the tailplane. Generalized curve.

As no other detailed analysis data is available the continuous curve as drawn in fig. 34 is assumed to apply for all conventional aircraft configurations. The curve is redrawn in fig. 35 in a generalised form.

As a further check on the validity of the procedure given above for the determination of the average dynamic pressure at the tail two further examples are presented.

In fig. 36 $\sqrt{q_h/q_o}$ as calculated and measured is presented for the DHC-5 Caribon in the clean configuration. The testdata were teken from ref. 47.

In fig. 37 $\sqrt{q_h/q_o}$ is presented for the Fokker 50 for three flap settings. The testdata were taken from unpublished windtunnel test data. Note how flap deflection lowers the position of the slipstream relative to the horizontail tailplane.

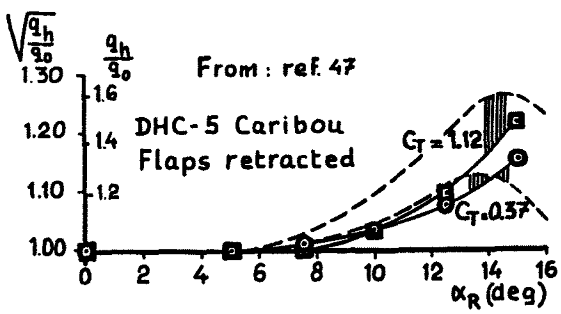

Figure 36 - Average dynamic pressure at the horizontal tail on the DHC-5 Caribou.

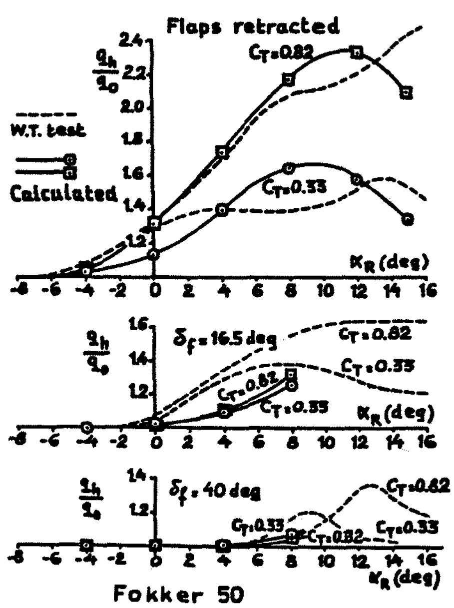

Figure 37 - Average dynamic pressure at the horizontal tail on the Fokker 50.

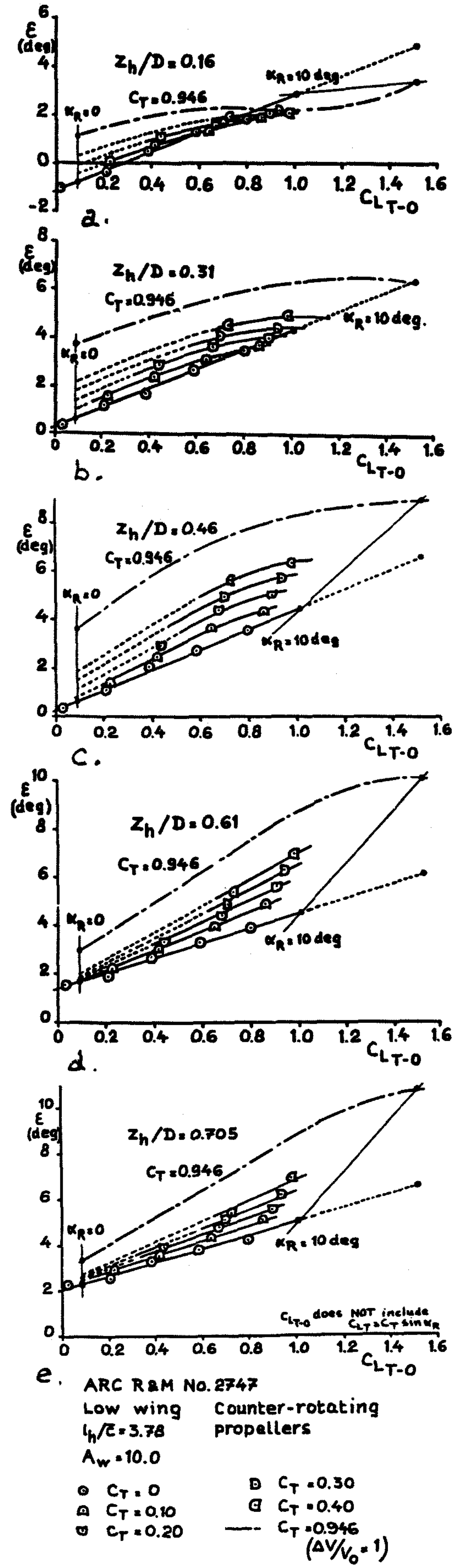

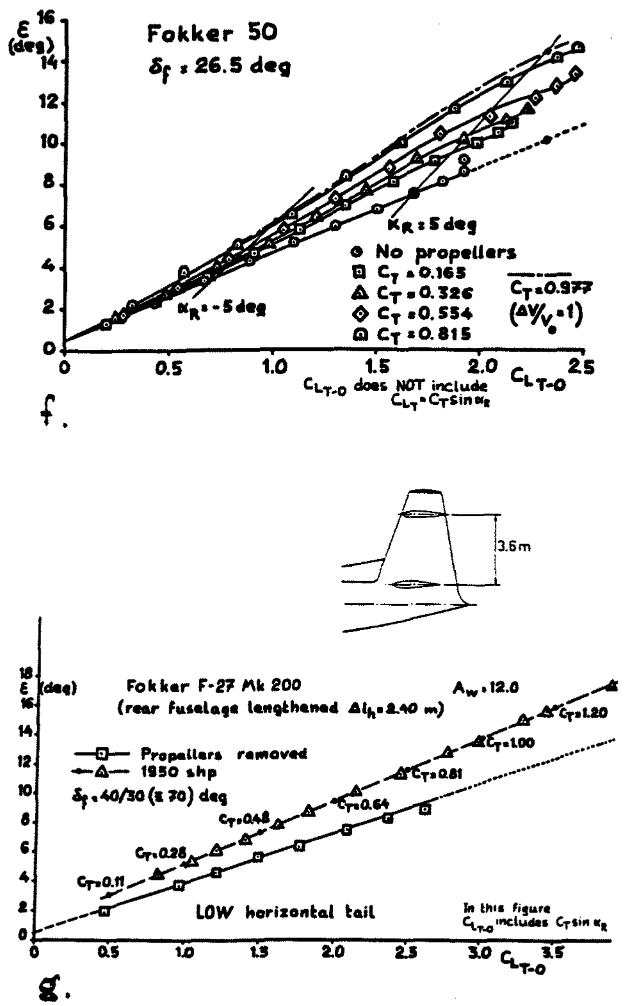

Figure 38 - Effect of the slipstream position on the average downwash angle at the horizontal tailplane.

6.4 The average downwash angle at the horizontal tailplane

In chapter 6.3 (and figs. 27, 28) it was shown that, when the horizontal tailplane lies sufficiently far above the propeller slipstream for practical purposes a single linear relationship can be assumed between the average downwash angle ε of the horizontal tailplane and the lift-coefficient for the aircraft-less-tail. Whether a given high lift coefficient is generated through a high angle-of-attack without slipstream or at a lower angle-of-attack combined with propeller slipstream, the same average downwash angle ε occurs.

When the distance between slipstream centre line and tailplane becomes less than one nominal slipstream diameter D^* this is no longer true however. In the mixing region on the boundary between slipstream and outer flow an inflow into the slipstream occurs which causes the average downwash to increase when the tailplane is located in that area. This is illustrated in fig. 38a to g. This inflow angle increases with increasing thrust coefficent. For the present analysis it has been assumed that $\Delta\varepsilon$ is proportional to $\Delta V/V_0$.

A large amount of available test data has been analysed on this extra downwash angle $\Delta\varepsilon$ above the increase in downwash directly related to the increase in wing lift due to slipstream.
When the testdata are normalised to a slipstream strength $\Delta V/V0 = 1$ the data points are shown to lie in a fairly narrow band as is illustrated in fig. 39. Note that the datapoints are not only taken from ref. 16 but also from refs. 7,21,36 and other sources. The background of fig. 39 is treated in more detail in ref. 49.
The drawn line in fig. 39 repeated in fig. 40 is the curve adopted for use in the present method for the determination of the downwash at the tailplane in the presence of propeller slipstream.

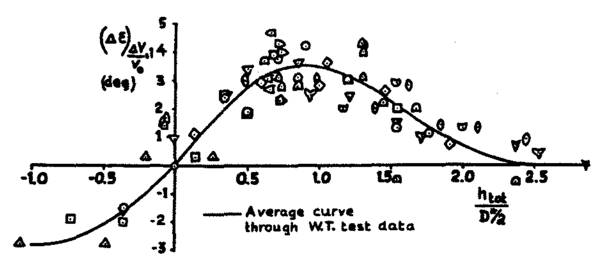

Figure 39 - Increase in downwash at the tailplane due to inflow into the slipstream.

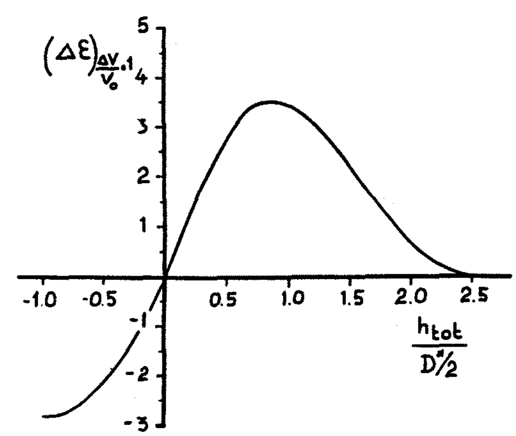

Figure 40 - Increase in downwash at the tailplane due to inflow into the slipstream. - Generalized curve.

The average downwash angle can then be written as:

$$\varepsilon = (\varepsilon_o)_{P-O} + \left[\frac{d\varepsilon}{dC_L}\right]_{P-O} \times C_{L_{W+S}} + (\Delta\varepsilon)_{\Delta V/V_o=1} \times \frac{\Delta V}{V_o}$$

The distance between slipstream centre line and tailplane, required to determine $(\Delta\varepsilon)_{\Delta V/V_o=1}$ is determined according to the procedure outlined in chapter 6.3.

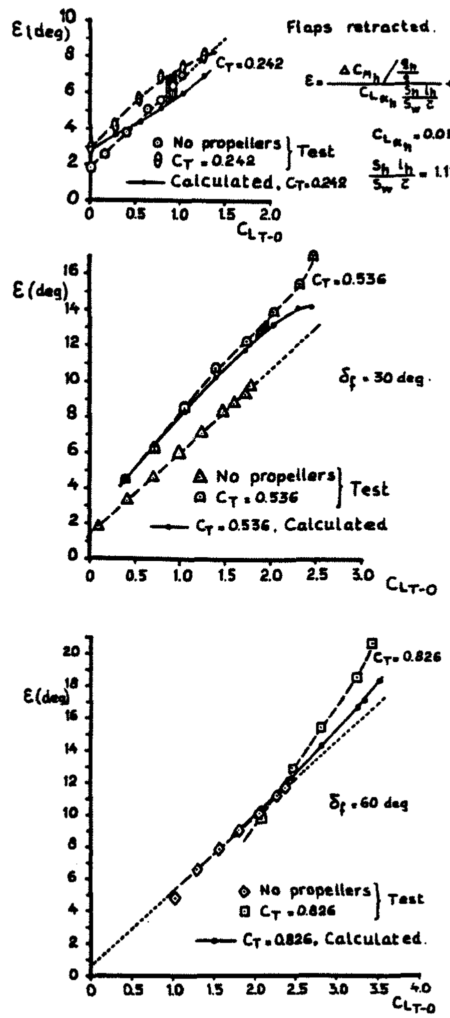

Figure 41 - Effect of propeller slipstream on the average downwash angle at the tailplane on the C-160 Transall. Comparison between theory and experiment.

Tail-on and tail-off windtunnel test data on the C-160 Transall with and without running propellers were analysed to compare downwash data as calculated according to the equation given above and as derived from the test data. The average dynamic pressure at the tail was calculated according to chapter 6.4. The comparison is presented in fig. 41. The effect of the vertical displacement of the slipstream due to flap deflection and the associated effect on the average downwash at the tail is clearly reproduced in the calculation.

7. Two examples of the decrease in longitudinal stability due to slipstream

Finally, the method to determine the effect of propeller slipstream on static longitudinal stability as described in the present report has been applied to the aircraft

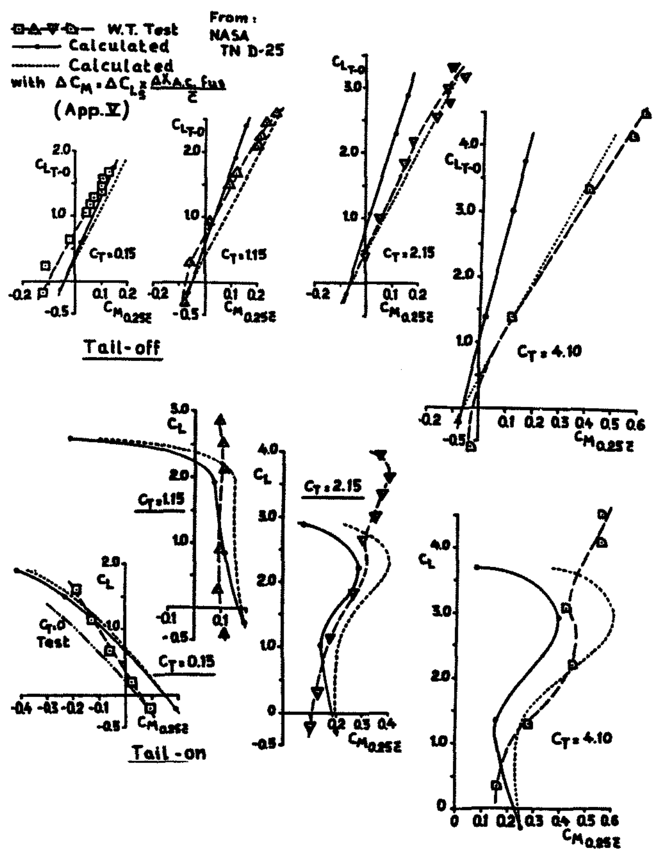

Figure 42 - Tail-off and tail-on pitching moment curves with flaps retracted. Comparison between theory and experiment.

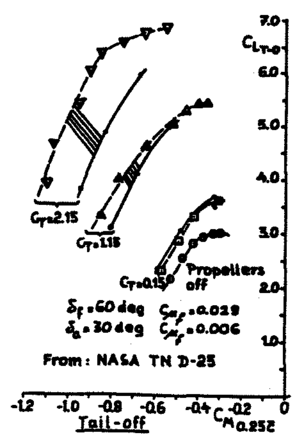

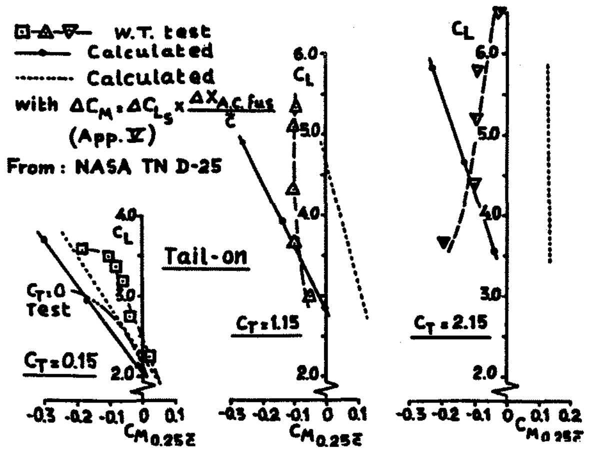

Figure 43 - Tail-off and tail-on pitching moment curves with flaps extended. Comparison between theory and experiment.

The aircraft configuration from refs. 36,37 with both flaps retracted and with flaps deflected 60 deg. and ailerons deflected 30 deg.
C_M-versus-C_L curves for the tail-off and tail-on configurations are presented in figs. 42, 43.
The tail-on curves were calculated according to the following equations valid for a given angle-of-attack, α_R and thrust coefficient C_T with horizontal tail setting i_h = 4.3 deg. and elevator in neutral position:

$$C_L = C_{L_{T-0}} + C_{L_{\alpha_h}}\left[\alpha_R\left(1-\frac{d\varepsilon}{dC_L}\left(\frac{dC_L}{d\alpha}\right)_{T-0}\right)-\varepsilon_{\alpha=0}+i_h\right]\times\frac{q_h}{q}\frac{S_h}{S_W}$$

$$C_{M_{CG}} = C_{M_{T-0}}$$

$$-C_{L_{\alpha_h}}\left[\alpha_R\left[1-\frac{d\varepsilon}{dC_L}\left(\frac{dC_L}{d\alpha}\right)_{T-0}\right]-\varepsilon_{\alpha=0}+i_h\right]\frac{q_h}{q}\frac{S_h}{S_w}\frac{l_h}{\bar{c}}$$

8. Conclusions

A method has been presented for the analysis of the effect of propeller slipstream on the static longitudinal stability and control of multi-engined aircraft. The method allows the determination of the increase in lift and the change in tail-off pitching moment due to slipstream, the location of the slipstream relative to the horizontal tailplane and the average downwash angle and dynamic pressure at the tailplane. A comparison of calculated and windtunnel test data showed the method to be suitable for preliminary design purposes.

9. Acknowledgement

The author gratefully acknowledges the assistance of Ms. Yvonne Spronk in the preparation of this paper.

References

1. Simmons, L.F.G. and Ower, E.: An investigation of downwash in the slipstream, ARC R&M No. 882, 1923

2. Bradfield, F.B. et al.: Windtunnel data on the effect of slipstream on the downwash and velocity at the tailplane, ARC R&M No. 1488, 1932.

3. Stüper, J.: Einfluss des Schraubenstrahls auf Flügel und Leitwerk, Luftfahrtforschung 1938, p. 181.

4. Glauert, H.: The lift and drag of a wing spanning a free jet, ARC R&M No. 1603, 1934.

5. Stüper, J.: Beitrag zum Problem des durch einen Freistrahl hindurch gesteckten Tragflugels, Luftfahrt forschung 1935, P. 267.

6. Smelt, R. and Davies, H.: Estimation of increase in lift due to slipstream, ARC R&M No. 1788, 1937

7. Bryant, L.W. and McMillan, G.A.: The longitudinal stability of a twin-engined monoplane with airscrews running, ARC R&M No. 2310, 1938.

8. Millikan C.B.: The influence of running propellers on airplane characteristics, Journal of the Aeronautical Sciences, Jan. 1940, p. 85

9. Falkner, V.M.; Nixon, H.L. and Sweeting, N.E.: An experimental investigation of the effect of airscrews on the longitudinal stability of a twin-engined monoplane, ARC R&M No. 2070, 1941

10. Schubert, R.: Zur Berechnung der statischen Längsstabilität im Motorflug, Luftfahrtforschung 1942, p. 271

11. Baranoff, von, A.; Beitrag zur Frage der Beeinflüssung des Abwindes durch den Schraubenstrahl, Luftfahrt forschung 1942, p 1.

12. Priestley, E.:
A general treatment of static longitudinal stability with propellers, with application to single-engined aircraft, ARC R&M No. 2732, 1944

13. Stiess, Von, W.:
Uber den Einfluss des Luftschraubendrehsinnes auf die Längsstabilität von zweimotorigen Flugzeugen, Jahrbuch 1938 der deutschen Luftfahrtforschung, p.206.

14. Katzoff, S.:
Longitudinal stability and control with special reference to slipstream effects,
NACA report No 690, 1940.

15. Spence, A.:
The effect of propeller thrust on downwash and velocity at tailplane. - A collection of data from low speed windtunnel tests, ARC Current Paper No 21, 1947.

16. Hartley, D.E.; Spence, A and Kirby, D.A.:
Model tests on the effect of slipstream on the flow at various tailplane positions on a four-engined aircraft, ARC R&M No. 2747, 1951.

17. Morris, D.E. and Morall, J.C.:
The effect of slipstream on the longitudinal stability of multi-engined aircraft,
ARC R&M 2701, 1948.

18. Draper, J.W. and Kuhn, R.E.:
Investigation of the aerodynamic characteristics of a model wing-propeller combination and of the wing and propeller separately at angles-of-attack up to 90°, NACA TN 3304, 1956 (Also NACA Report 1263).

19. Kuhn, R.E. and Grunwald, K.J.:
Longitudinal aerodynamic characteristics of a four-propeller deflected slipstream VTOL model including the effects of ground proximity.
NASA TN D-248, 1960.

20. Weiberg, J.A. and Holzhauser C.A.:
Large-scale windtunnel tests of an airplane model with an unswept, tilt wing of aspect ratio 5.5 and with four propellers and blowing flaps.
NASA TN D-1034, 1961.

21. Margason, R.J.; Hammond, A.D. and Gentry, G.L.:
Longitudinal stability and control characteristics of a powered model of a twin-propeller deflected-slipstream STOL aircraft configuration.
NASA TN D-3438, 1966.

22. Page, V.R.; Dickinson, S.O. and Deckert, W.H.:
Large-scale windtunnel tests of a deflected slipstream STOL model with wings of various aspect ratio's.
NASA TN D-4448, 1968.

23. Page, V.R. and Aiken, T.N.:
Stability and control characteristics of a large-scale deflected slipstream STOL model with a wing of 5.7-aspect ratio. NASA TN D-6393, 1971.

24. De Young, J.:
Propeller at high incidence, Journal of Aircraft, May-June 1965, p. 241.

25. Strand, T.; Levinsky, E.S. and Wei, H.Y.:
Unified performance theory for V/STOL aircraft in equilibrium flight, Journal of Aircraft, 1967.

Part I : March-April 1967, p. 105
Part II: May-June 1967, p. 193

26. Levinsky, F.S.; Thommen, H.U.; Yager, P.M. and Holland, C.H.: Lifting surface theory for V/STOL aircraft in transition and cruise.
Journal of Aircraft,
1969-1970.
Part I , Nov.-Dec. 1969, p. 488
Part II , Jan.-Febr. 1970, p. 58

27. Fowler, H.D.:
Determination of the influence of propeller thrust on C_L and C_D of an airplane using a triple-slotted flap at various deflections.
SAE Paper No 690724, 1969.

28. Brenckmann, M.:
Experimental investigation of the aerodynamics of a wing in a slipstream,
University of Toronto, UTIA Technical Note No. 11, 1957
Also in: Journal of the Aeronautical Sciences, May 1958.

29. Ribner, H.S.:
Theory of wings in slipstreams, University of Toronto, UTIA Technical Note No. 60, 1959.

30. Ellis, N.D.:
A computer study of a wing in a slipstream, University of Toronto, UTIA Technical Note

No. 101, 1967.

31. Jameson, A.:
Analysis of wing slipstream flow interaction.
NASA CR-1632, 1970.

32. Rethorst, S.:
Aerodynamics of Non-uniform flows as related to an airfoil extending through a circular jet, Journal of the Aeronautical Sciences, 1958.

33. Fink, M.P.; Cocke, B.W. and Lipson, S.:
A wind-tunnel investigation of a 0.4-scale model of an assault-transport airplane with boundary-layer control applied,
NACA RM L55G26a, 1955.

34. Weiberg, J.A.; Griffin, R.N. and Florman, G.L.:
Large-scale wind-tunnel tests of an airplane model with an unswept, aspect-ratio-10 wing, two propellers, and area-suction flaps,
NACA TN 4365, 1958.

35. Griffin, R.N.; Holzhauser, C.A. and Weiberg, J.A.:
Large-scale windtunnel tests of an airplane model with an unswept, aspect-ratio-10 wing, two propellers, and blowing flaps.
NASA Memo 12-3-58A, 1958.

36. Weiberg, J.A. and Page, V.R.:
Large-scale windtunnel tests of an airplane model with an unswept, aspect-ratio-10 wing, four propellers, and blowing flaps.
NASA TN D-25, 1959.

37. Weiberg, J.A. and Holzhauser, C.A.:
STOL characteristics of a propeller-driven, aspect-ratio-10, straight-wing airplane with boundary-layer control flaps, as estimated from large-scale windtunnel tests.
NASA TN D-1032, 1961

38. Kuhn, R.E.:
Semi-empirical procedure for estimating lift and drag characteristics of propeller-wing-flaps configurations for vertical- and short-take-off-and-landing airplanes.
NASA Memo 1-16-59A, 1958.

39. Eliraz, Y.:
Aircraft power-on polars corrected for propeller slipstream deflection, Israel Journal of Technology, Vol. 9 Nos 1-2, 1971, p. 195.

40. Marr, R.L.:
A method for analyzing Power-on static longitudinal stability, SAE Paper No 700238, 1970.

41. Segall, R.N. and Gajdjis, S.:
An enhanced method for reducing power-on lift coefficent data to power-off lift coefficient data for multi-engined propeller aircraft.
AIAA Paper No. 91-0683, 1991.

42. Jones, R.T.:
Properties of low-aspect-ratio pointed wings at speeds below and above the speed of sound,
NACA report 835, 1946.

43. De Young, J.:
Spanwise loading for wings and control surfaces of low aspect ratio, NACA TN 2011, 1949.

44. Stepniewski, W.Z.:
Expérience tirée des essais en vol d'un appareil VTOL à aile basculante. Technique et Science Aeronautiques, 1960, No. 1, p. 1.

45. Glauert, H.:
Theoretical relationships for an airfoil with hinged flap, ARC R&M No. 1095, 1927.

46. Abbott, I.H. and Doenhoff, von, A.E.: Theory of wing section, Dover Publications, Inc, New York, 1958, p. 215.

47. Nettleton, T.R.:
Handling qualities research in the development of a STOL utility transport aircraft, Canadian Aeronautical and Space Journal, March 1966, p. 93.

48. Borne, van den, P.C.M. and Hengst, van, J.:
Investigation of propeller slipstream effects on the Fokker 50 through in-flight pressure measurements,
AAIAA Paper No. 90-3084, 1990.

49. Obert, E.:
A method for the determination of the effect of propeller slipstream on static longitudinal stability and control of multi-engined aircraft.
Delft University of Technology, LR - 761 ,1994.

50. Verweij, A.:
A preliminary design study of an aircraft equipped with two high-power, wing mounted tractor propeller engines with special emphasis on longitudinal and lateral stability and control.
Thesis, Delft University of Technology, June 1992.

Appendix I

The total lift on a lifting surface with running propellers

According to lifting line theory the lift on a wing with elliptic lift distribution can be written as:

$$L_W = \dot{m}_o\, V_o \sin \varepsilon = \rho \frac{\pi}{4}\, b_W^2\, V_o^2 \sin \varepsilon$$

where ε is the average downwash of the flow over the wing infinitely far behind the wing. The flow can thus be considered as s stream tube with circular cross section and diameter b_W which is deflected downward over an angle ε. This model is now assumed to apply to any conventional wing shape.
The lift due to slipstream is also considered to be equal to the momentum resulting from the downward deflection over an angle ε_S of each slipstream tube with fully contracted diameter D^*.
where:

$$D^* = D \sqrt{\frac{V_o + \Delta V/2}{V_o + \Delta V}}$$

The lift due to slipstream can then be written as:

$$L_S = n_e\, \dot{m}_s\, (V_o + \Delta V) \sin \varepsilon_S = n_e\, \rho\, \frac{\pi}{4}\, D^*\, (V_o + \Delta V)^2 \sin \varepsilon_S$$

On a lifting wing with slipstream present the cross-sectional area from the slipstream tubes has to be subtracted from the cross-sectional area of the stream tube describing the outer flow (see fig. 1). The total wing lift then becomes:

$$L_{W+S} = \rho\, V_o^2 \left[\frac{\pi}{4}\, b_W^2 - n_e\, \frac{\pi}{4} D^{*2}\right] \sin \varepsilon + \rho\, [V_o + \Delta V]^2\, n_e \frac{\pi}{4} D^{*2} \sin \varepsilon_S$$

and:

$$C_{L_{W+S}} = \frac{L_{W+S}}{\frac{1}{2}\rho V_o^2 S_W} = \frac{2}{S_W}\left(\frac{\pi}{4} b_W^2 - n_e \frac{\pi}{4} D^{*2}\right) \sin\varepsilon + \frac{F}{T} n_e \frac{\pi D^{*2}}{2 S_W} \frac{(V_o + \Delta V)^2}{V_o^2} \sin\varepsilon_S$$

where the factor $\frac{F}{T}$ is discussed at the end of this appendix.

When the propeller thrust is parallel to the fuselage reference line the total propeller thrust can be written as: (see fig. Ia).

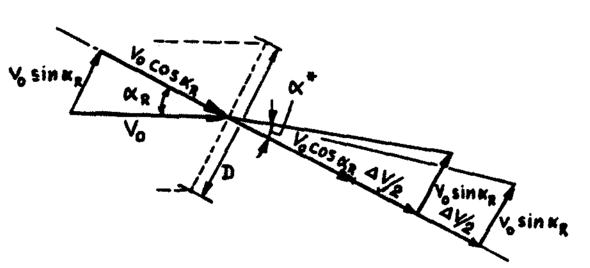

Figure Ia

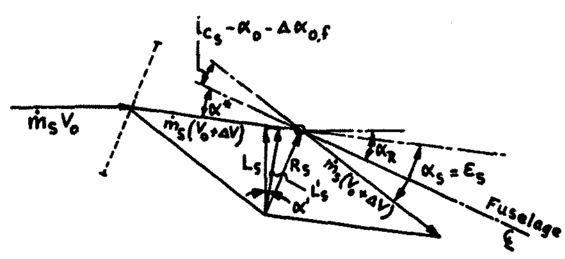

Figure Ib

$$T = C_T \frac{1}{2} \rho \, V_O^2 \, S_W = \dot{m}_S \, \Delta V = \rho \left[V_O \cos \alpha_R + \frac{\Delta V}{2} \right] \frac{\pi}{4} D^2 \cos \alpha_R \, \Delta V$$

and the downwash angle far behind the propeller: $\varepsilon_p = \alpha_R - \alpha^*$

where $\alpha^* = arctg \dfrac{V_O \sin \alpha_R}{V_O \cos \alpha_R + \Delta V}$

An extensive comparison between calculated and measured increase in lift due to slipstream showed a much better correlation when α^* was written as:

$$\alpha^* = arctg \frac{V_O \sin \alpha_R}{V_O \cos \alpha_R + \Delta V/2}$$

This means the downwash behind the propeller is considered at the propeller disc. This definition of α^* is used in all further calculations.

For the wing part covered by the slipstream the average effective angle-of- attack relative to the fuselage reference line is equal to α^*.
However the aerodynamic angle-of-attack measured from the zero-lift line is:

$$\alpha_S = \alpha^* + i_{c_s} - \alpha_O - \Delta\alpha_{O,f}$$

where: i_{Cs} = angle of incidence of the local wing chord relative to the fuselage reference line.
α_O = zero-lift angle-of-attack relative to the chord line of the airfoil section at the propeller axis location.
$\Delta\alpha_{0,f}$ = change in zero-lift angle-of-attack due to flap deflection

$$\Delta\alpha_{O,f} = - \frac{dc_l/d\delta}{dc_l/d\alpha} \times \delta_{f_{eff}}$$

As discussed in the main text the lift due to slipstream is considered to be equal to the lift on a wing with aspect ratio $A_{S,eff}$ in a free stream with velocity $V = V_O + \Delta V$.

$$\sin \varepsilon_S = \frac{2 \, C_{L_{s,eff}}}{\pi \, A_{S,eff}} \sin \alpha_S$$

If $A_{S,eff} \leq 1.5$ then $A_{S,eff} \approx \pi/2 \, A_S$ and $\sin \varepsilon_S = \sin \alpha_S$

Note that strictly speaking C_{L_s} should be determined as indicated in fig. Ib.

However for small values of $\alpha' = (\alpha - \alpha_s + \varepsilon_s/2)$ the difference between R_S and L_S can be neglected. In the examples presented in this paper and ref. 49 this difference has consistently been neglected. At very large angles-of-attack and very high C_T-values this may no longer be acceptable.

Kuhn has shown that at large flap deflections momentum losses occur in the slipstream, possibly due to viscous effects. Fig. Ic shows the curves adopted in the present method for the factor F/T as a function of flap setting for various flap types to account for these momentum losses.

For the total increase in lift due to running propellers the vertical thrust component

$$L_T = C_T \frac{1}{2} \rho \, V_O^2 \, S_W \sin \alpha_R$$

and the total propeller normal force

$$L_P = C_{L_P} \frac{1}{2} \rho V_0^2 S_W$$

has to be added to the total wing lift. C_{L_P} is determined according to the method presented in ref. 24.

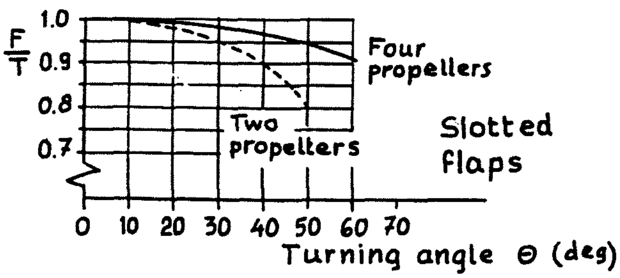

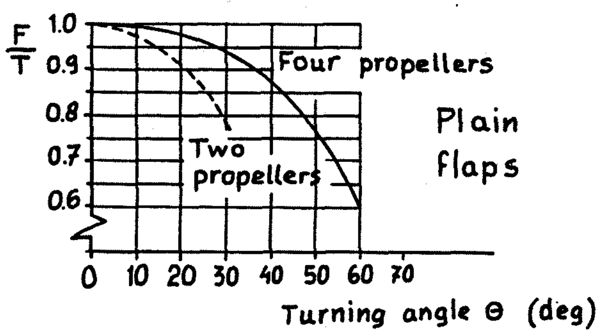

Figure IC

Appendix II

Estimation of the lift due to slipstream for the configuration analysed in ref. 28. (UTIA TN No 11)

In report UTIA TN No 11 a parameter σ was defined:

$$\sigma = \frac{\bar{q}_{jet}/q_0 - 1}{\bar{q}_{jet}/q_0 + 1} \quad \textit{where jet = slipstream}$$

This can also be written as:

$$\frac{\bar{q}_j}{q_0} = \frac{1+\sigma}{1-\sigma}$$

For $\Delta V/V_0 = 0$ the total lift can be written as $L_{tot} = L_W + L_S$.

$$\textit{Then: } \Delta L_S = [L_W + L_S]_{\frac{\Delta V}{V_0} \neq 0} - [L_W]_{\frac{\Delta V}{V_0} = 0}$$

With the equations from Appendix I this can be written as:

$$\Delta L_S = \rho\, [V_0 + \Delta V]^2 \frac{\pi}{4} D^{*2} \sin \varepsilon_S - \rho V_0^2 \frac{\pi}{4} D^{*2} \sin \varepsilon$$

The thrust $T = \rho \frac{\pi}{4} D^{*2} [V_0 + \Delta V]\, \Delta V$ and $\dfrac{\Delta L_S}{T} = \dfrac{[V_0+\Delta V]^2 \sin \varepsilon_S - V_0^2 \sin \varepsilon}{(V_0 + \Delta V)\, \Delta V}$

As the model under consideration is a 2-dim. model $\varepsilon = 0$.

$$\textit{So: } \frac{\Delta L_S}{T} = \frac{(V_0+\Delta V)^2 \sin \varepsilon_S}{(V_0+\Delta V)\, \Delta V} = \left[\frac{V_0}{\Delta V} + 1\right] \sin \varepsilon_S$$

As $D = 8$ in, $c = 8$ in, $b = 32$ in it is assumed again that $\varepsilon_S = \alpha_S$. and as the propeller is not attached to the model and fixed in the tunnel $\alpha_S = \alpha$.

So: $\dfrac{\Delta L_S}{T} = \left[\dfrac{V_0}{\Delta V} + 1\right] \sin \alpha$ and $\left[\dfrac{V_0}{\Delta V} + 1\right] = \dfrac{\Delta L_S}{T \sin \alpha}$

As $\frac{1+\sigma}{1-\sigma}=\frac{q_j}{q_o}=\left[1+\frac{\Delta V}{V_o}\right]^2$ a unique relation exists between σ, $V_o/\Delta V$ and $\frac{\Delta L_s}{T \sin\alpha}$
In the following table some numerical values are presented

σ	$V_o/\Delta V$	$\frac{\Delta L_s}{T \sin}$
1.00	0	1.00
0.88	0.338	1.338
0.76	0.586	1.586
0.62	0.947	1.947
0.49	1.410	2.410
0.26	3.289	4.289

A comparison between these calculated data and windtunnel test results is presented in figs. 11a, b.

Appendix III

The theoretical average dynamic pressure at the horizontal tail of multi-engined propeller aircraft

The effect of propeller slipstream on the theoretical average dynamic pressure at the tail q_h, is considered under the following assumptions:

1. The slipstream is fully contracted at the tail location.

2. The slipstream cross-section is circular with diameter D^*.
   No mixing on the slipstream boundary occurs nor any deformation of the cross-section. The average dynamic pressure in the slipstream is:

   $$q_s=\frac{1}{2}\rho V_o^2\left[1+\frac{\Delta V}{V_o}\right]^2$$

   The average dynamic pressure at the tailplane location is:

   $$q_h=\frac{1}{2}\rho V_o^2\left[1+\left(\frac{\Delta V}{V_o}\right)_{av}\right]^2=\frac{1}{2}\rho V_o^2\ (1+b)^2$$

   According to fig. III a the width of the tailplane part covered by the slipstream of a single propeller is:

   $$b_s=2\sqrt{\left[\frac{D^*}{2}\right]^2-h_{tot}^2}$$

   or:

   $$b_s=D^*\sqrt{1-\left[\frac{h_{tot}}{D^*/2}\right]^2}$$

The tail area covered by the slipstream of two propellers is:

$$S_s = 2 \times b_s \times c_s$$

The average dynamic pressure at the tail is then:

$$\frac{1}{2}\rho\,(1+b)^2\,V_o^2 = \frac{1}{2}\rho\left[1+\frac{\Delta V}{V_o}\right]^2 V_o^2\,S_s + V_o^2\,[S_h - S_s]$$

or:

$$(1+b)^2 = \left[1+\frac{\Delta V}{V_o}\right]^2 \frac{S_s}{S_h} + \frac{S_h - S_s}{S_h}$$

Then:

$$b = \sqrt{\left[1+\frac{\Delta v}{V_o}\right]^2 \frac{S_s}{S_h} + \frac{S_h - S_s}{S_h}} - 1$$

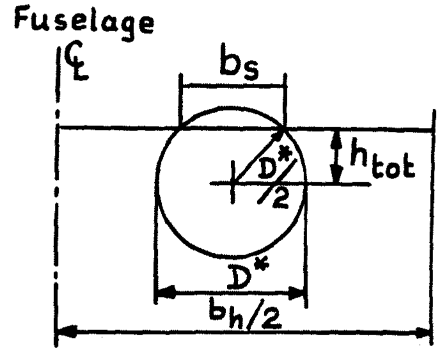

Figure IIIa

and

$$b_{max} = \sqrt{\left[1+\frac{\Delta V}{V_o}\right]^2 \frac{2 \times D^* \times c_s}{S_h} + \frac{S_h - 2 \times D^* \times c_s}{S_h}} - 1$$

For the configuration from report ARC R&M No 2747 (ref. 16) b has been calculated as a function of $h_{tot}/D^*/2$ for $C_T = 0.40$.

$$\frac{\Delta V}{V_o} = 0.506;\quad D^* = 9.12\quad ;S_h = 197.3\,sq.\quad ;c_s = 5.80$$

The result is shown as the broken curve in fig. 34. This figure illustrates that the estimated location of the slipstream centre line is correct. Slipstream spread and deformation does occur however. The curve for b to be used in the method described in the present report is also indicated in fig. 34.

Appendix IV

The theoretical average downwash angle at the horizontal tailplane behind a wing with running propellers

It is assumed that the average downwash angle at the tail of a multi-engined propeller aircraft is determined by the combined effects of lift due to wing angle-of-attack and due to slipstream.

As before, the lift of a wing with slipstream is considered to be equivalent to the sum of the vertical components of the outgoing momentum of a stream tube determined by the wing span and of the stream tubes determined by the fully contracted propeller slipstream.

The cross-sectional area of the basic wing lift stream tube is then devided in a central part with area A^* determined by the outer edges of the two inboard fully contracted slipstream diameters and the two outerparts with total cross-sectional area 2A.

These area's can be written as

$$2A = 2\left[\frac{\emptyset}{2}\,\frac{b_w^2}{4} - \frac{b_w}{2}\cos\emptyset \times J\right] \qquad \text{or} \qquad 2A = 2\,\frac{b_w^2}{4}\left[\frac{\emptyset}{2} - \cos\emptyset\left[Y_{s_o} + D^*/2\right]\right]$$

then

$$A = \varnothing \times \frac{b_w^2}{4} - \frac{b_w}{2}\cos\varnothing \; \frac{Y_{s_o} + D^*/2}{b_w/2}$$

or

$$A = \frac{b_w^2}{4}\,[\varnothing - \sin\varnothing\cos\varnothing]$$

and

$$\varnothing = \arccos \frac{Y_{s_o} + D^*/2}{b_w/2}$$

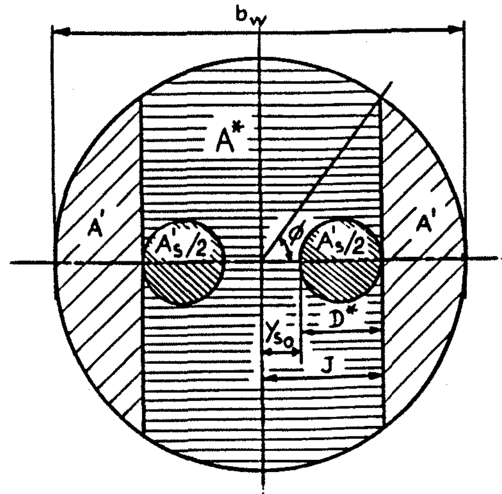

Figure IV a

The slipstream cross sectional area is: $A'_S = n_e \frac{\pi}{4} D^{*2} = 2 \times \frac{\pi}{4} D^{*2}$

$$A^* = \frac{\pi}{4} b_w^2 - \frac{b_w^2}{4}(\varnothing - \sin\varnothing\cos\varnothing) - \frac{\pi}{2} D^{*2}$$

Then:
It is now assumed that the mutual interference between slipstream and outer flow results in the same average downwash angle for both slipstream and the central part of the outer flow with area A^* determined by the addition of both the vertical components of the outgoing momentum and of the mass flow of the three stream tubes with cross sectional area's A^* and A_S .
So,

$$\sin\varepsilon' = \frac{\rho V_0^2 A^* \sin\varepsilon + \rho (V_o + \Delta V)^2 A'_S \sin\varepsilon_s}{\rho V_0^2 A^* + \rho (V_o + \Delta V)^2 A'_S}$$

For the configuration from report NASA TN D-25 (ref. 36) with flaps deflected to 60 deg and ailerons to 30 deg the average downwash angle ε' was determined for both power-off conditions and for C_T = 2.15. With
$D^*/2$ = 0.60 m , $b_w/2$ = 6.86 m , Y_{So} = 3.09 m, then ϕ = 57.46 deg.
ϕ
The lift was calculated according to the method described in the main body of this paper. This lead to the following results:

	$C_T = 0$	$C_T = 2.35$
$\alpha_R = 0$	: C_L = 2.75 ; ε = 10.2 deg	C_L = 4.81 ; ε' = 16.0 deg
α_R = 8 deg	: C_L = 3.35 ; ε = 12.5 deg	C_L = 5.58 ; ε' = 18.9 deg

In fig. 30 a comparison is shown between calculated and actual test data.
The assumption that slipstream and outer flow have identical average downwash angles seems to hold.

Note that the decrease in average downwash at the horizontal tail location which occurs when the tail is moved further away from the wing-wake/slipstream centre line remains. This account for the difference in actual downwash angle obtained from theory and windtunnel tests.

Appendix V

NOTES

1. When the tried thrust contribution to the pitching moment ΔC_{M_T} is considered not the thrust coefficient C_T but the effective thrust coefficient $C_{T_{eff}}$ has to be taken. $C_{T_{eff}}$ is defined as

$$C_{T_{eff}} = C_T - \Delta C_T$$ where ΔC_T is a measure for the increase in wing drag due to slipstream. On the basis of the data presented in refs. 33-37 and under the assumption that $\Delta C_T = \Delta C_D$ due to slipstream figure Va was prepared.

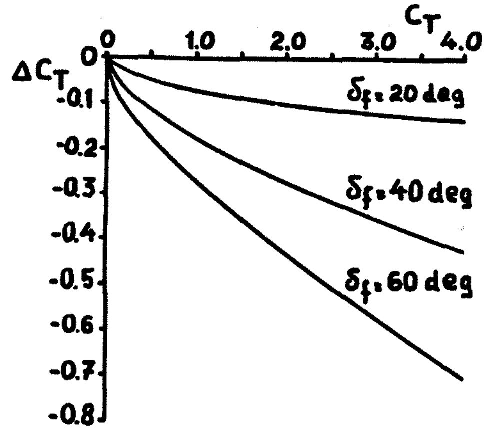

Figure Va

2. When figures 42 and 43 were prepared it was noticed that better agreement between calculated and test data was obtained when the pitching moment contribution from the fuselage due to the upwash in front of the wing was extended to the increase in lift due to slipstream. Then, at a given angle-of-attack the following pitching moment contribution has to be added to the pitching moment calculated with the formulae given in the main part of this paper:

$$\Delta C_M = \Delta C_{L_s} \times \Delta \frac{X_{ac.fus}}{\bar{C}}$$

where $\Delta \frac{X_{ac.fus}}{\bar{C}}$ is the forward shift in aerodynamic centre due to the presence of the fuselage.

It is unclear however if the above applies in a general form and further investigation is required on this subject.

Appendix VI

Aircraft configurations considered in the main body of this paper